

# Transition state geometry near higher-rank saddles in phase space

George Haller<sup>1</sup>, T Uzer<sup>2</sup>, Jesús Palacián<sup>3</sup>, Patricia Yanguas<sup>3</sup> and Charles Jaffé<sup>4</sup>

<sup>1</sup> Department of Mechanical Engineering and Department of Mathematics and Statistics, McGill University, Montreal, QC H3A 2K6, Canada

<sup>2</sup> Center for Nonlinear Sciences, School of Physics, Georgia Institute of Technology, Atlanta, GA 30332-0430, USA

<sup>3</sup> Departamento de Ingeniería Matemática e Informática, Universidad Pública de Navarra, 31006 Pamplona, Spain

<sup>4</sup> Department of Chemistry, West Virginia University, Morgantown, WV 26506-6045, USA

E-mail: [cjaffe@wvu.edu](mailto:cjaffe@wvu.edu)

Received 19 August 2009, in final form 3 November 2010

Published 7 January 2011

Online at [stacks.iop.org/Non/24/527](http://stacks.iop.org/Non/24/527)

Recommended by B Leimkuhler

## Abstract

We present a detailed analysis of invariant phase space structures near higher-rank saddles of Hamiltonian systems. Using the theory of pseudo-hyperbolic invariant surfaces, we show the existence of codimension-one normally hyperbolic invariant manifolds that govern transport near the higher-rank saddle points. Such saddles occur in a number of problems in celestial mechanics, chemical reactions, and atomic physics. As an example, we consider the problem of double ionization of helium in an external electric field, a basis of many modern ionization experiments. In this example, we illustrate our main results on the geometry and transport properties near a rank-two saddle.

Mathematics Subject Classification: 37C75, 37D10, 37J40, 70H09, 81V45, 78A35

 Online supplementary data available from [stacks.iop.org/Non/24/527/mmedia](http://stacks.iop.org/Non/24/527/mmedia)

(Some figures in this article are in colour only in the electronic version)

## 1. Introduction

In the theory of chemical reactions the rates and product distributions are determined by the bottlenecks that restrict transport in the classical phase space [1–3]. In the simplest case a single bottleneck exists and is associated with a fixed point that is stable in all but one degree

of freedom. In other words, the fixed point corresponds to a simple or rank-one saddle [2]. In more complicated situations additional bottlenecks can occur. They can be arranged in series, parallel or some combination thereof. Again, geometrically these bottlenecks correspond to rank-one saddles. If the bottlenecks occur in series, then the rate of reaction is given by the flux through the most restrictive bottleneck. On the other hand, when there is more than a single possible outcome to a reaction, the bottlenecks occur in parallel and the rates and product distributions will be governed by relative limiting rates associated with the bottlenecks in the various paths leading from reactants to products.

The question of the existence and relevance of saddles with rank greater than one has interested chemists for decades [4–10]. Few concrete results exist in this challenging subject. One of the earliest, the Murrell–Laidler theorem [4, 5], implies that the reaction path, that is, the path of steepest descent, will not pass through a saddle of rank two or greater. The proof of this theorem, for rank-two saddles, is based upon the existence of a path on the potential energy surface that connects two minima with a maximum energy less than that of the rank-two saddle. This path passes through a rank-one saddle with less energy than the rank-two saddle. Note that the minima may correspond to reactants, intermediates or products and may be either local or global minima. The extension of this theorem to saddles of higher rank is straightforward.

The placement of these minima is clearly determined by the rank-one saddles. Similarly, rank-two saddles are responsible for the placement of the rank-one saddles. To make this clear, consider two rank-one saddles that are connected by a ridge. Following this ridge from one saddle to the other, there will be a point of maximum energy. This point corresponds to a saddle of rank two. These arguments can be extended to higher order; two rank- $n$  saddles will be connected by a ridge; the point of maximum energy along this ridge will correspond to a rank- $(n + 1)$  saddle.

Unfortunately the role of higher-rank saddles, beyond that of the ordering of the lower-rank saddles, remains obscure. For the most part this is because attention has focused on the morphology of the potential energy surface (often called the energy landscape) whereas questions concerning transport are properly formulated in the classical phase space. For years the same issue has hindered progress in the identification of the transition state, namely the true surface of no return, in systems having more than two degrees of freedom [1–3].

We have recently reported in these pages [2] a formalism that enabled us to construct, for the first time, the higher-dimensional geometrical structures that regulate the transport from the reactants to the product regimes. These structures, which include dividing surfaces, separatrices and transition states, lie at the heart of the theory of reaction dynamics as developed by chemists and is known as transition state theory [11–16]. While this theory was initially developed in the study of chemical [11] and nuclear [12] reactions, in retrospect one recognizes that it can be applied in much broader situations ranging from the transport of small masses in the solar system [17, 18], through chemistry [3, 19] and atomic physics [20–23] to the dynamics of nucleons within the nucleus [24].

In this paper we use these same techniques to explore the phase space geometry of saddles of rank greater than one. In the next section we review our previous work with regard to transport across rank-one saddles and outline the difficulties that occur when it is applied to situations involving saddles of higher rank. In the third section we turn our attention to saddles of higher rank ( $n \geq 2$ ). Here we prove the existence of surfaces of codimension one that can be used to partition the energy shell and to characterize the transport in phase space. In section 4 we apply these results to a prominent problem from atomic physics, the correlated double ionization of helium in an external electric field [25]. This event takes place through the Stark saddle which is of rank two. We summarize our results in section 5.

## 2. Rank-one saddles

Consider a Hamiltonian  $H(p, q)$  having  $n$  degrees of freedom [2]. The state or phase space of this system will be  $2n$ -dimensional, having both a coordinate and momentum for each degree of freedom. The dynamics of the system are determined by Hamilton's equations of motion, a set of  $2n$  first-order differential equations. The phase flow is governed by the occurrence of bottlenecks associated with fixed points defined as

$$\begin{aligned}\dot{p}_i &= -\frac{\partial H(p_1, \dots, p_n, q_1, \dots, q_n)}{\partial q_i} = 0, \\ \dot{q}_i &= \frac{\partial H(p_1, \dots, p_n, q_1, \dots, q_n)}{\partial p_i} = 0\end{aligned}$$

for  $i = 1, \dots, n$ . Of particular importance are fixed points that are unstable in the first degree of freedom and stable in the remaining  $(n - 1)$  degrees of freedom. These fixed points correspond to simple or rank-one saddles. In what follows the first degree of freedom is assumed to be the unstable, or reactive, degree of freedom.

The geometry of these points is relatively simple. In the immediate vicinity of the fixed point, which is taken as the origin, the Hamiltonian can be shown to have the form [2]

$$H(p, q) = \frac{1}{2}(p_1^2 - \lambda_1^2 q_1^2) + \frac{1}{2} \sum_{i=2}^n (p_i^2 + \omega_i^2 q_i^2) + f(I_1, p_2, \dots, p_n, q_2, \dots, q_n),$$

where  $f(I_1, p_2, \dots, p_n, q_2, \dots, q_n) = \mathcal{O}(q_i^k p_j^l)$ ,  $k + l \geq 3$ ,  $\lambda_1 > 0$  and  $I_1 = \frac{1}{2}(p_1^2 - \lambda_1^2 q_1^2)$ .

The equations of motion are given by

$$\dot{p}_1 = \left(1 + \frac{1}{\lambda_1} \frac{\partial f}{\partial I_1}\right) \lambda_1^2 q_1, \quad \dot{q}_1 = \left(1 + \lambda_1 \frac{\partial f}{\partial I_1}\right) p_1$$

and

$$\dot{p}_i = -\omega_i^2 q_i - \frac{\partial f}{\partial q_i}, \quad \dot{q}_i = p_i + \frac{\partial f}{\partial p_i}$$

for  $i = 2, \dots, n$ .

Note that if  $p_1 = q_1 = 0$  then  $\dot{p}_1 = \dot{q}_1 = 0$ . This set of conditions defines a  $(2n - 2)$ -dimensional invariant manifold

$$C = \left\{ (p, q) \in \mathbb{R}^{2n} : \frac{1}{2} \sum_{i=2}^n (p_i^2 + \omega_i^2 q_i^2) + f(0, p_2, \dots, p_n, q_2, \dots, q_n), q_1 = 0, p_1 = 0 \right\}.$$

This is the centre manifold of the fixed point at the origin. Taking the intersection of this manifold with the energy shell

$$\mathcal{E}_h = \{(p, q) \in \mathbb{R}^{2n} : H(p, q) = h > 0\}$$

defines a  $(2n - 3)$ -dimensional *normally hyperbolic invariant manifold* (NHIM)

$$\begin{aligned}C_h = \mathcal{E}_h \cap C = & \left\{ (p, q) \in \mathbb{R}^{2n} : \frac{1}{2} \sum_{i=2}^n (p_i^2 + \omega_i^2 q_i^2) \right. \\ & \left. + f(0, p_2, \dots, p_n, q_2, \dots, q_n) = h > 0, q_1 = 0, p_1 = 0 \right\}.\end{aligned}$$

The NHIM is the fundamental object in the theory of transport through the phase space bottleneck. It possesses a pair of stable and unstable manifolds,

$$W^s(C_h) = \left\{ (p, q) \in \mathbb{R}^{2n} : \frac{1}{2} \sum_{i=2}^n (p_i^2 + \omega_i^2 q_i^2) \right. \\ \left. + f(0, p_2, \dots, p_n, q_2, \dots, q_n) = h > 0, p_1 = -\lambda_1 q_1 \right\},$$

$$W^u(C_h) = \left\{ (p, q) \in \mathbb{R}^{2n} : \frac{1}{2} \sum_{i=2}^n (p_i^2 + \omega_i^2 q_i^2) \right. \\ \left. + f(0, p_2, \dots, p_n, q_2, \dots, q_n) = h > 0, p_1 = \lambda_1 q_1 \right\}.$$

Each of these manifolds can be partitioned into two parts, a forward part and a backward part,

$$W_f^s(C_h) = \left\{ (p, q) \in \mathbb{R}^{2n} : \frac{1}{2} \sum_{i=2}^n (p_i^2 + \omega_i^2 q_i^2) \right. \\ \left. + f(0, p_2, \dots, p_n, q_2, \dots, q_n) = h > 0, p_1 = -\lambda_1 q_1 \geq 0 \right\},$$

$$W_f^u(C_h) = \left\{ (p, q) \in \mathbb{R}^{2n} : \frac{1}{2} \sum_{i=2}^n (p_i^2 + \omega_i^2 q_i^2) \right. \\ \left. + f(0, p_2, \dots, p_n, q_2, \dots, q_n) = h > 0, p_1 = \lambda_1 q_1 \geq 0 \right\},$$

$$W_b^s(C_h) = \left\{ (p, q) \in \mathbb{R}^{2n} : \frac{1}{2} \sum_{i=2}^n (p_i^2 + \omega_i^2 q_i^2) \right. \\ \left. + f(0, p_2, \dots, p_n, q_2, \dots, q_n) = h > 0, p_1 = -\lambda_1 q_1 \leq 0 \right\},$$

$$W_b^u(C_h) = \left\{ (p, q) \in \mathbb{R}^{2n} : \frac{1}{2} \sum_{i=2}^n (p_i^2 + \omega_i^2 q_i^2) \right. \\ \left. + f(0, p_2, \dots, p_n, q_1, \dots, q_n) = h > 0, p_1 = \lambda q_1 \leq 0 \right\}.$$

The forward and backward parts of these two manifolds

$$W_f(C_h) = W_f^s(C_h) \cup W_f^u(C_h),$$

$$W_b(C_h) = W_b^s(C_h) \cup W_b^u(C_h)$$

join to yield two  $(2n - 2)$ -dimensional invariant tubes that, respectively, correspond to the forward and backward reactive tubes [26–33]. They are embedded in the  $(2n - 1)$ -dimensional energy shell and hence are codimension one surfaces. Consequently, the states within these

tubes remain confined to the tubes and flow from the interior of  $W_j^s$  into the interior of  $W_j^u$  (where  $j = f$  or  $b$ ) [2]. It should be noted that the intersection of the forward (backward) tubes is just the NHIM

$$\begin{aligned} C_h &= W_f^s(C_h) \cap W_f^u(C_h), \\ C_h &= W_b^s(C_h) \cap W_b^u(C_h). \end{aligned}$$

Two transition states can now be defined as cross-section surfaces in each of the forward and backward reactive tubes,

$$\begin{aligned} \text{TS}_f(C_h) &= \left\{ (p, q) \in \mathbb{R}^{2n} : \frac{1}{2} p_1^2 + \frac{1}{2} \sum_{i=2}^n (p_i^2 + \omega_i^2 q_i^2) \right. \\ &\quad \left. + f(I_1, p_2, \dots, p_n, q_2, \dots, q_n) = h > 0, q_1 = 0, p_1 \geq 0 \right\}, \\ \text{TS}_b(C_h) &= \left\{ (p, q) \in \mathbb{R}^{2n} : \frac{1}{2} p_1^2 + \frac{1}{2} \sum_{i=2}^n (p_i^2 + \omega_i^2 q_i^2) \right. \\ &\quad \left. + f(I_1, p_2, \dots, p_n, q_2, \dots, q_n) = h > 0, q_1 = 0, p_1 \leq 0 \right\}. \end{aligned}$$

These are, respectively, the forward and backward transition states. Their union is a  $(2n - 2)$ -dimensional sphere ( $q_1 = 0$ ) and their intersection is simply the NHIM (a  $(2n - 3)$ -dimensional sphere). And finally, we observe that all states exterior to the two reactive tubes do not react, that is, they are confined to either reactant or product regions of phase space for all time.

### 2.1. Extension to higher-rank saddles

The question immediately arises: Can similar arguments be applied to the case of higher-rank saddles? The simple answer is that they can be applied but do not yield impenetrable barriers in the energy shell [1] and, consequently, are of little interest in the study of transport. Consider a Hamiltonian system having  $n$  degrees of freedom and possessing a fixed point corresponding to a rank- $m$  saddle. The centre manifold will be  $(2n - 2m)$ -dimensional, its intersection with the energy shell will be a  $(2n - 2m - 1)$ -dimensional NHIM. This NHIM will possess stable and unstable manifolds. These manifolds will be of dimension  $(2n - 2m)$  or equivalently of codimension  $(2m - 1)$  in the energy shell. Clearly, only in the case of a rank-one saddle  $m = 1$  do these geometrical constructs provide impenetrable barriers. Similarly, the transition states are also of codimension- $(2m - 1)$  and thus will not partition the energy shell into reactant and product regions.

The question remains as to whether or not these arguments can be modified so as to define impenetrable barriers in the cases of saddles having rank greater than one. This is the subject of the rest of this paper. In summary, new ideas are needed to construct transport barriers near higher-rank saddles. The rest of this paper is devoted to this subject.

## 3. Higher-rank saddles

Our focus here is the Hamiltonian flow geometry in the vicinity of a rank- $m$  saddle. The linearized flow geometry is integrable, and hence its codimension-one transport barriers can be located explicitly. Unlike in the rank-one case, however, extending these barriers to the

full nonlinear system cannot be accomplished through classic normally hyperbolic invariant manifold theory [34] because of the unboundedness of the barriers.

The classic theory of normally hyperbolic invariant manifolds only applies to compact manifolds such as spheres. This is not merely a technicality: unbounded invariant manifolds will, in general, not persist under the addition of the nonlinear terms. Hence, there is no immediately applicable result that would guarantee the nonlinear continuation of the non-compact set  $C_h$  or of its stable and unstable manifolds.

Our discussion concludes with a theorem identifying conditions under which nonlinear analogs of the linear transport barriers exist near higher-rank saddles. Instead of using normally hyperbolic invariant manifold theory, we rely on ideas from the theory of pseudo-hyperbolic invariant manifolds.

### 3.1. Phase space geometry for linearized Hamiltonian flow

Consider the quadratic Hamiltonian

$$H_2(p, q) = \frac{1}{2} \sum_{i=1}^m (p_i^2 - \lambda_i^2 q_i^2) + \frac{1}{2} \sum_{i=m+1}^n (p_i^2 + \omega_i^2 q_i^2). \quad (1)$$

The origin  $p = 0, q = 0$  admits  $(n - m)$  elliptic directions within the centre subspace  $E^c$ ; rotations within this subspace are governed by the  $(n - m)$  frequencies  $\omega_i$ . The origin also has an  $m$ -dimensional stable subspace  $E^s$  and an  $m$ -dimensional unstable subspace  $E^u$ .

Exponential growth and decay in  $E^s \times E^u$  is governed by the eigenvalues  $\{\lambda_i\}_{i=1}^m$  and  $\{-\lambda_i\}_{i=1}^m$ , respectively, of the linear Hamiltonian system generated by (1). We assume that the largest eigenvalue is  $\lambda_1$  is strictly positive, and the rest are ordered in the fashion

$$-\lambda_1 < -\lambda_2 \leq \dots \leq -\lambda_m \leq 0 \leq \lambda_m \leq \lambda_{m-1} \leq \dots \leq \lambda_2 < \lambda_1. \quad (2)$$

Observe that  $\lambda_1$  is assumed strictly larger than  $\lambda_2$ . For the rank-one saddles, one has  $\lambda_2 = -\lambda_2 = 0$ . The eigenvalue configuration and the phase space structure for the Hamiltonian (1) is sketched in figure 1.

*3.1.1. Strong stable and unstable subspaces.* We define two invariant subspaces within each of  $E^s$  and  $E^u$  by writing

$$E^s = E_1^s \times \widehat{E}^s, \quad E^u = E_1^u \times \widehat{E}^u. \quad (3)$$

Here the *strong stable subspace*,  $E_1^s$ , is the invariant subspace spanned by the eigenvector corresponding to the exponent  $-\lambda_1$ . Similarly, the *strong unstable subspace*  $E_1^u$  is spanned by the eigenvector corresponding to  $\lambda_1$ . As seen from (3), the  $(m - 1)$ -dimensional invariant subspace  $\widehat{E}^s$  is the span of the eigenvectors corresponding to the eigenvalues  $-\lambda_2, \dots, -\lambda_m$ . Solutions in this subspace decay to the origin no faster than  $\exp(-\lambda_2 t)$ . Similarly, the  $(m - 1)$ -dimensional invariant subspace  $\widehat{E}^u$  is the span of the eigenvectors corresponding to the eigenvalues  $\lambda_2, \dots, \lambda_m$ . Solutions in this subspace grow no faster than  $\exp(\lambda_2 t)$ .

*3.1.2. Pseudo-stable and pseudo-unstable subspaces.* We now define the  $\lambda_2$ -unstable subspace of the origin,  $E_{\lambda_2}^u$ , as the maximal invariant subspace in which the norm of solutions grows, stays constant, or decays no faster than  $\exp(-\lambda_2 t)$ . Note that  $E_{\lambda_2}^u$  is a  $(2n - 1)$ -dimensional subspace of the form

$$E_{\lambda_2}^u = E^c \times \widehat{E}^s \times E^u, \quad (4)$$

and contains all eigenvectors of the linearized Hamiltonian flow except for the one corresponding to the strong stable subspace  $E_1^s$ . For this reason, we also refer to  $E_{\lambda_2}^u$  as a

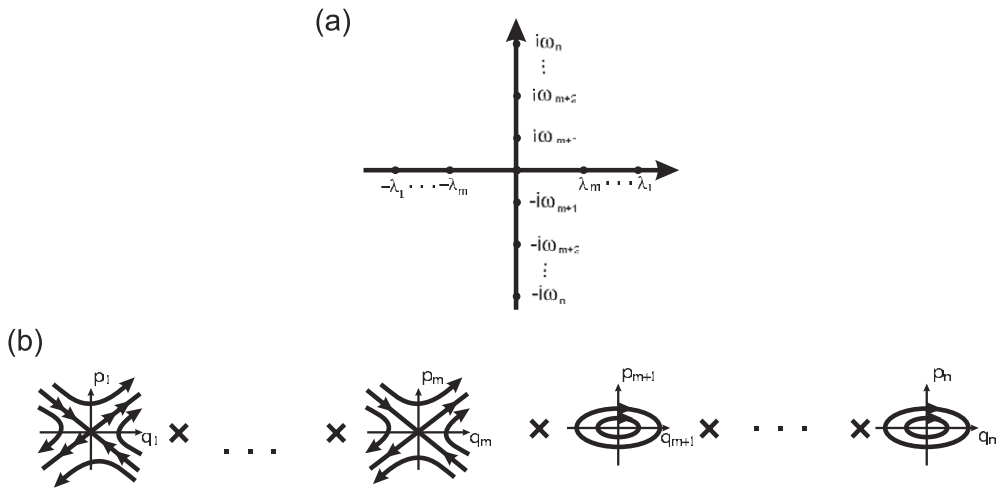


**Figure 1.** The (a) eigenvalue configuration and (b) phase space structure for the quadratic Hamiltonian  $H_2$ .

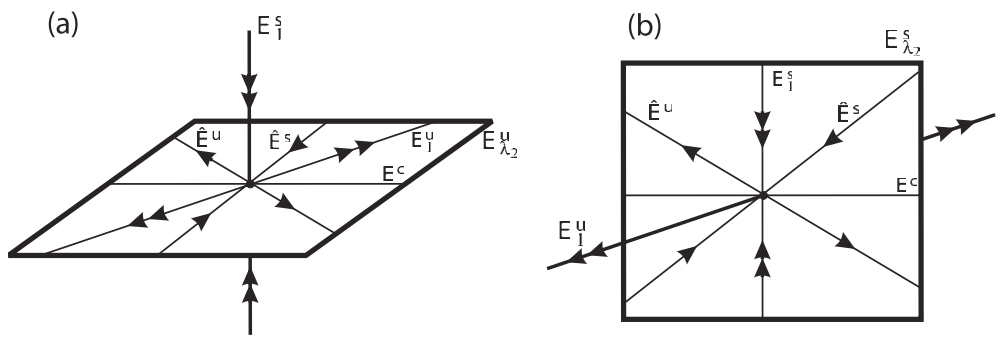


**Figure 2.** The geometry of the (a) pseudo-unstable and (b) pseudo-stable subspaces.

pseudo-unstable subspace, because although it contains stable directions as well, these stable directions are weaker than the strong stable dynamics in  $E_1^s$ . This property renders  $E_{\lambda_2}^u$  to be a codimension one normally hyperbolic invariant manifold for the quadratic Hamiltonian  $H_2$ . The geometry of  $E_{\lambda_2}^u$  is sketched in figure 2.

Similarly, we define the  $\lambda_2$ -stable subspace,  $E_{\lambda_2}^s$ , as the maximal invariant subspace in which the norm of solutions decays, stays constant, or grows no faster than  $\exp(\lambda_2 t)$ . Note that  $E_{\lambda_2}^s$  is also a  $(2n - 1)$ -dimensional subspace of the form

$$E_{\lambda_2}^s = E^c \times E^s \times \hat{E}^u,$$

often called a *pseudo-stable subspace*. This subspace is also a codimension one normally hyperbolic invariant manifold for the quadratic Hamiltonian  $H_2$ . The geometry of  $E_{\lambda_2}^s$  is also sketched in figure 2.

Note that both the pseudo-stable and the pseudo-unstable subspaces are normally hyperbolic invariant manifolds, i.e. stretching and contraction rates in the direction transverse to them dominates stretching and contraction rates in directions tangent to them. Due to their non-compactness, however, these manifolds are not unique: there are infinitely many other manifolds whose geometric and dynamic properties are similar to those of  $E_{\lambda_2}^s$  and  $E_{\lambda_2}^u$ .

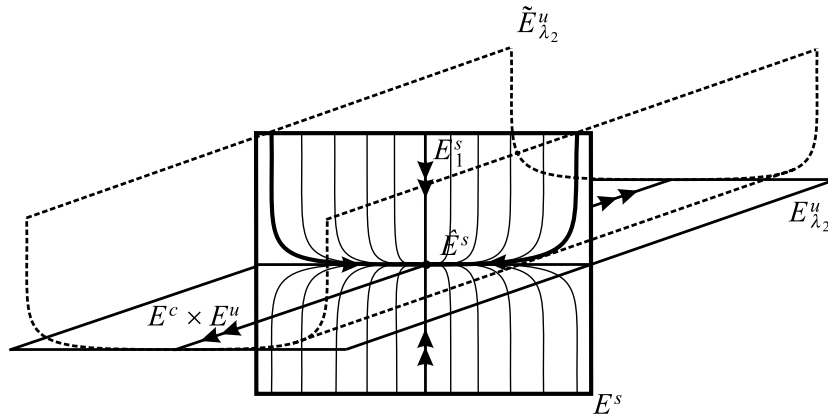


**Figure 3.** Non-uniqueness of the pseudo-unstable manifold  $E^u_{\lambda_2}$ . Note that the manifold  $\tilde{E}^u_{\lambda_2}$  has the same asymptotic and geometric features as  $E^u_{\lambda_2}$  does.

For instance, there are infinitely many smooth invariant surfaces that are (1) tangent to  $E^u_{\lambda_2}$  at the origin, (2) contain solutions that do not decay to the origin in backward time faster than  $\exp(-\lambda_2 t)$  and (3) do not grow in forward time faster than  $\exp(\lambda_1 t)$ . These manifolds intersect the stable subspace  $E^s$  in solutions that are tangent to  $\hat{E}^s$ . The non-uniqueness of the pseudo-unstable manifold  $E^u_{\lambda_2}$  is illustrated in figure 3.

While the pseudo-unstable manifold  $E^u_{\lambda_2}$  and the pseudo-stable manifold  $E^s_{\lambda_2}$  are not unique, they are normally hyperbolic, as noted above. This property makes them *a priori* more robust under perturbations of  $H_2$  than other subspaces. For instance, the span of all eigenvectors of the linearized Hamiltonian flow except for the one corresponding to  $\lambda_2$  is also a codimension one invariant subspace, but is not normally hyperbolic, because the growth rate  $\exp(\lambda_1 t)$  inside this subspace is stronger than the growth rate  $\exp(\lambda_2 t)$  transverse to this subspace. As a result, this subspace is not expected to survive under general perturbations to the Hamiltonian  $H_2$ .

**3.1.3. Transition state geometry for the linearized Hamiltonian flow.** Unlike classic stable and unstable subspaces, the pseudo-stable and pseudo-unstable subspaces,  $E^s_{\lambda_2}$  and  $E^u_{\lambda_2}$ , are not disjoint: their intersection is the  $(2n - 2)$ -dimensional subspace

$$C = E^s_{\lambda_2} \cap E^u_{\lambda_2} = E^c \times \hat{E}^s \times \hat{E}^u$$

that contains all centre directions, as well as the weaker stable and unstable directions. The geometry of the normally hyperbolic invariant manifold  $C$  is shown in figure 4.

Consider now the intersections of  $C$  with the quadratic energy surface

$$\mathcal{E}_h = \{(p, q) \in \mathbb{R}^{2n} : H_2(p, q) = h > 0\}.$$

This intersection,

$$C_h = \mathcal{E}_h \cap C = \left\{ (p, q) \in \mathbb{R}^{2n} : \frac{1}{2} \sum_{i=2}^m (p_i^2 - \lambda_i^2 q_i^2) + \frac{1}{2} \sum_{i=m+1}^n (p_i^2 + \omega_i^2 q_i^2) = h > 0, q_1 = 0, p_1 = 0 \right\},$$

is, strictly speaking, not normally hyperbolic: it has a neutrally stable direction normal to the energy surface. The set  $C_h$  is, however, normally hyperbolic within the energy surface  $\mathcal{E}_h$ .

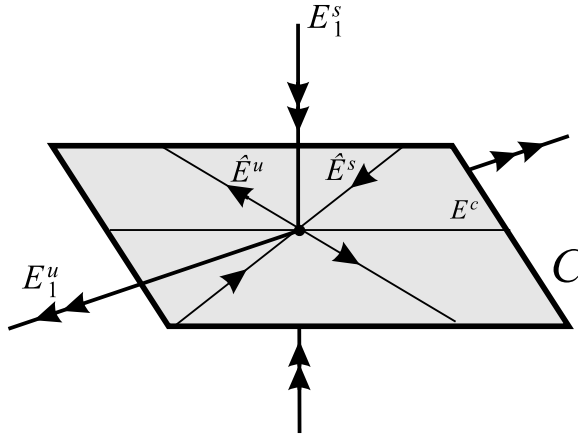


Figure 4. The geometry of the normally hyperbolic invariant manifold  $C$ .

We will call  $C_h$  the pseudo-NHIM and reserve the term NHIM for the intersection of the centre manifold with the energy shell. It is important to recognize that the pseudo-NHIM  $C_h$  is not bounded and consequently classic normally hyperbolic invariant manifold theory is not applicable [34]. This is reflected in the fact that, geometrically,  $C_h$  is diffeomorphic to near-critical energy surfaces of a Hamiltonian with a rank- $(m - 1)$  saddle. Such a near-critical energy surface contains  $S^{2n-2m}$  (a saddle-type invariant sphere), as well as the stable and unstable manifolds of this sphere, which are each diffeomorphic to  $S^{2n-2m} \times \mathbb{R}^{m-1}$ .

The surface  $C_h$  is a  $(2n - 3)$ -dimensional manifold. It has codimension one (i.e.  $(2n - 2)$ -dimensional) stable and unstable manifolds within the energy surface  $\mathcal{E}_h$ , given by

$$W^s(C_h) = \left\{ (p, q) \in \mathbb{R}^{2n} : \frac{1}{2} \sum_{i=2}^m (p_i^2 - \lambda_i^2 q_i^2) + \frac{1}{2} \sum_{i=m+1}^n (p_i^2 + \omega_i^2 q_i^2) = h > 0, \quad p_1 = -\lambda_1 q_1 \right\}, \quad (5)$$

$$W^u(C_h) = \left\{ (p, q) \in \mathbb{R}^{2n} : \frac{1}{2} \sum_{i=2}^m (p_i^2 - \lambda_i^2 q_i^2) + \frac{1}{2} \sum_{i=m+1}^n (p_i^2 + \omega_i^2 q_i^2) = h > 0, \quad p_1 = \lambda_1 q_1 \right\}. \quad (6)$$

These manifolds can be partitioned into a forward part and a backward part, given by

$$W_f^s(C_h) = \left\{ (p, q) \in \mathbb{R}^{2n} : \frac{1}{2} \sum_{i=2}^m (p_i^2 - \lambda_i^2 q_i^2) + \frac{1}{2} \sum_{i=m+1}^n (p_i^2 + \omega_i^2 q_i^2) = h > 0, \quad p_1 = -\lambda_1 q_1 \geq 0 \right\},$$

$$W_f^u(C_h) = \left\{ (p, q) \in \mathbb{R}^{2n} : \frac{1}{2} \sum_{i=2}^m (p_i^2 - \lambda_i^2 q_i^2) + \frac{1}{2} \sum_{i=m+1}^n (p_i^2 + \omega_i^2 q_i^2) = h > 0, \quad p_1 = \lambda_1 q_1 \geq 0 \right\},$$

$$W_b^s(C_h) = \left\{ (p, q) \in \mathbb{R}^{2n} : \frac{1}{2} \sum_{i=2}^m (p_i^2 - \lambda_i^2 q_i^2) + \frac{1}{2} \sum_{i=m+1}^n (p_i^2 + \omega_i^2 q_i^2) = h > 0, \quad p_1 = -\lambda_1 q_1 \leq 0 \right\},$$

$$W_b^u(C_h) = \left\{ (p, q) \in \mathbb{R}^{2n} : \frac{1}{2} \sum_{i=2}^m (p_i^2 - \lambda_i^2 q_i^2) + \frac{1}{2} \sum_{i=m+1}^n (p_i^2 + \omega_i^2 q_i^2) = h > 0, \quad p_1 = \lambda_1 q_1 \leq 0 \right\}.$$

The forward and backward parts of these two manifolds join to form two  $(2n - 2)$ -dimensional invariant sets

$$W_f(C_h) = W_f^s(C_h) \cup W_f^u(C_h),$$

$$W_b(C_h) = W_b^s(C_h) \cup W_b^u(C_h).$$

We call  $W_f(C_h)$  the forward-reacting tube and  $W_b(C_h)$  the backward-reacting tube [26–33]. They are embedded in the  $(2n - 1)$ -dimensional energy shell and hence are codimension one. Consequently, the states within these tubes remain confined to the tubes and flow from the interior of  $W_j^s$  into the interior of  $W_j^u$  (where  $j = f$  or  $b$ ) [2].

We can define two transition states globally for the linearized Hamiltonian flow by  $H_2$ . These transition states are cross-section surfaces in each of the forward and backward reactive tubes, defined as

$$\text{TS}_f(C_h) = \left\{ (p, q) \in \mathbb{R}^{2n} : \frac{1}{2} p_1^2 + \frac{1}{2} \sum_{i=2}^m (p_i^2 - \lambda_i^2 q_i^2) + \frac{1}{2} \sum_{i=m+1}^n (p_i^2 + \omega_i^2 q_i^2) = h > 0, \quad q_1 = 0, \quad p_1 \geq 0 \right\},$$

$$\text{TS}_b(C_h) = \left\{ (p, q) \in \mathbb{R}^{2n} : \frac{1}{2} p_1^2 + \frac{1}{2} \sum_{i=2}^m (p_i^2 - \lambda_i^2 q_i^2) + \frac{1}{2} \sum_{i=m+1}^n (p_i^2 + \omega_i^2 q_i^2) = h > 0, \quad q_1 = 0, \quad p_1 \leq 0 \right\}.$$

These are, respectively, the forward and backward transition states. Their union is a  $(2n - 2)$ -dimensional unbounded surface and their intersection is the pseudo-NHIM,  $C_h$ . We sketch the geometry of the forward and backward transition states for the quadratic Hamiltonian  $H_2$  in figure 5.

### 3.2. Phase space geometry for the full Hamiltonian flow

We now extend the geometry described above for the linearized Hamiltonian flow to the full nonlinear system. Near the origin  $p = 0, q = 0$ , the full  $n$  degrees of freedom Hamiltonian can be written in the form

$$H(p, q) = \frac{1}{2} \sum_{i=1}^m (p_i^2 - \lambda_i^2 q_i^2) + \frac{1}{2} \sum_{i=m+1}^n (p_i^2 + \omega_i^2 q_i^2) + f(I_1, p_2, \dots, p_n, q_2, \dots, q_n) \quad (7)$$

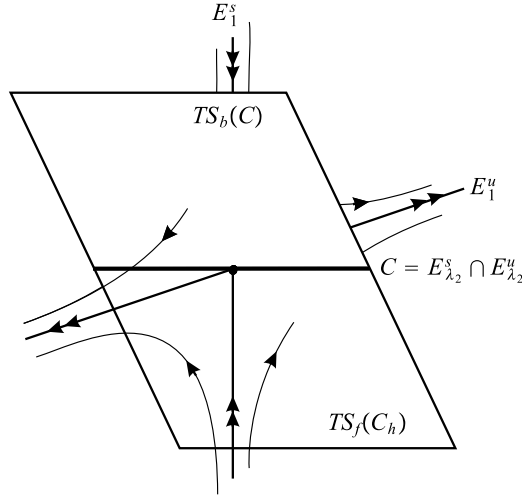


**Figure 5.** The forward and backward transition states,  $TS_f(C)$  and  $TS_b(C)$ , respectively. The transition states within the energy surface  $\{H_2 = h\}$  are obtained by taking the intersection of  $TS_f(C)$  and  $TS_b(C)$  with that energy surface.

where  $f(I_1, p_2, \dots, p_n, q_2, \dots, q_n) = \mathcal{O}(q_i^k p_j^l)$ ,  $k + l \geq 3$  and  $I_1 = (1/2\lambda_1)(p_1^2 - \lambda_1^2 q_1^2)$ . More specifically,  $f$  denotes a  $C^{r+1}$  function with  $r \geq 1$ . If  $H(p, q)$  does not have the form of (7), one needs to apply normal-form theory to transform the Hamiltonian into this form. It can be achieved if the ratios of the eigenvalues  $\lambda_1/\lambda_j$  with  $j = 2, \dots, m$  are not rational or close to rational (see [appendix A](#)).

For the Hamiltonian flow generated by  $H$ , we seek nonlinear continuations of the stable and unstable manifolds of  $C_h$  in each energy surface. Unlike in the rank-one saddle case, the extension of such surfaces cannot be concluded from classic normally hyperbolic invariant manifold theory [34]. The primary reason for this is the non-compactness of the set  $C_h$ . Even if we intersect  $C_h$  with a bounded ball centred at the origin, the resulting intersection is neither in-flowing nor out-flowing invariant, and hence Fenichel's classic results from [34] cannot be invoked to conclude the persistence of the intersection set under the addition of higher-order terms to the Hamiltonian.

To circumvent this problem, we focus on the nonlinear continuation of the pseudo-stable and pseudo-unstable subspaces,  $E_{\lambda_2}^s$  and  $E_{\lambda_2}^u$ . Their continuation turns out to exist under condition (2): we refer to a nonlinear continuation of  $E_{\lambda_2}^s$  as a pseudo-stable manifold  $W^{ps}(0)$  of the origin; a nonlinear continuation of  $E_{\lambda_2}^u$  is called a pseudo-unstable manifold  $W^{pu}(0)$  of the origin. We sketch the geometry of the pseudo-unstable manifold in figure 6.

The manifolds  $W^{ps}(0)$  and  $W^{pu}(0)$  are invariant, but not necessarily as smooth as the Hamiltonian flow map

$$\begin{aligned} \mathcal{P}^t: \mathbb{R}^{2n} &\rightarrow \mathbb{R}^{2n}, \\ (p_0, q_0) &\mapsto (p(t), q(t)). \end{aligned}$$

In contrast to classical stable and unstable manifolds, most solutions in  $W^{ps}(0)$  do not tend to the origin in forward time, and most solutions in  $W^{pu}(0)$  do not tend to the origin in backward time. Solutions in  $W^{ps}(0)$ , however, can only grow at speeds slightly above  $\exp(\lambda_2 t)$  while they are close to the origin. Likewise, solutions in  $W^{pu}(0)$  can only grow in backward time at speeds slightly above  $\exp(\lambda_2 t)$  while they are in the vicinity of the origin.

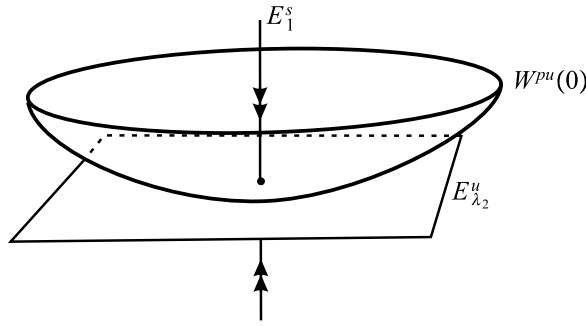


**Figure 6.** The geometry of the pseudo-unstable manifold  $W^{pu}(0)$ .

We have seen that even  $E_{\lambda_2}^s$  and  $E_{\lambda_2}^u$  are non-unique in terms of their main defining properties. As a result, pseudo-stable and -unstable manifolds are also non-unique. This means that there will be infinitely many invariant manifolds with the above properties, all tangent to  $E_{\lambda_2}^s$  and  $E_{\lambda_2}^u$  at the origin, but departing more and more from each other away from the origin. The following theorem summarizes the main properties of the pseudo-stable and pseudo-unstable manifolds.

**Theorem 1.** Assume that condition (2) holds, and define the constant

$$\bar{r} = \min(\text{Int}[\lambda_1/\lambda_2], r), \quad (8)$$

with  $\text{Int}[\cdot]$  referring to the integer part of a number; recall that  $r \geq 1$  is the degree of smoothness for the Hamiltonian  $H$  defined in (7). Then the  $p = q = 0$  fixed point of the full Hamiltonian  $H$  admits a (non-unique)  $(2n - 1)$ -dimensional class  $C^{\bar{r}}$  pseudo-stable manifold  $W^{ps}(0)$  and a (non-unique)  $(2n - 1)$ -dimensional class  $C^{\bar{r}}$  pseudo-unstable manifold  $W^{pu}(0)$ ; these manifolds are tangent to the subspaces  $E_{\lambda_2}^s$  and  $E_{\lambda_2}^u$ , respectively, at the origin.

If the function  $\mathcal{P}^t(p, q)$  is small enough globally in the  $C^{\bar{r}+1}$  norm (which can always be achieved by smoothly deforming the Hamiltonian outside a small enough neighbourhood of the origin), then for the constant

$$a = \exp[(\lambda_2 + \lambda_1/\text{Int}[\lambda_1/\lambda_2])/2],$$

we have

$$W^{ps}(0) = \left\{ (p, q) \in \mathbb{R}^{2n} : \sup_{t \geq 0} |\mathcal{P}^t(p, q)| a^{-t} < \infty \right\}, \quad (9)$$

i.e.  $W^{ps}(0)$  consists of solutions that grow at most at the rate  $a^t$ . Similarly,

$$W^{pu}(0) = \left\{ (p, q) \in \mathbb{R}^{2n} : \sup_{t \leq 0} |\mathcal{P}^t(p, q)| a^{-t} < \infty \right\}. \quad (10)$$

**Proof.** The existence of  $W^{ps}(0)$  and  $W^{pu}(0)$  with the above properties can be proved by applying Irwin's theorem [35, 36] on pseudo-stable manifolds in the current context. We spell out the details for  $W^{ps}(0)$ ; the proof being identical for  $W^{pu}(0)$  in backward time.

First, note that for any fixed  $t > 0$ , the splitting  $E_{\lambda_2}^s \oplus E_1^u$  of  $\mathbb{R}^{2n}$  is invariant under the linearized time-map  $D\mathcal{P}^t(0)$ . The estimates

$$\|D\mathcal{P}^t(0)\|_{E_{\lambda_2}^s} = e^{\lambda_2 t} < a, \quad (11)$$

and

$$\|D\mathcal{P}^t(0)\|_{E^u}^{-1} = e^{-\lambda_1} < a^{-\rho} \tag{12}$$

hold simultaneously for some constant  $a > 0$  and integer  $\rho \geq 1$ , whenever

$$e^{\lambda_2} < a < e^{\lambda_1/\rho}. \tag{13}$$

Such a constant  $a > 0$  always exists if we select

$$\rho = \text{Int} [\lambda_1/\lambda_2]. \tag{14}$$

In that case, the choice of

$$a = \exp [(\lambda_2 + \lambda_1/\text{Int} [\lambda_1/\lambda_2]) / 2] \tag{15}$$

ensures that (13) holds.

Conditions (11) and (12) are precisely the two main conditions of Irwin’s theorem in [35]. As a result, whenever (14) holds, Irwin’s theorem guarantees the existence of a (non-unique) class- $\mathcal{C}^\rho$  pseudo-stable invariant manifold  $W^{ps}(0)$  that is tangent to the subspace  $E_{\lambda_2}^s$  at the origin. To be precise, the degree  $\bar{r}$  of smoothness of  $W^{ps}(0)$  is the minimum of  $r$ , the smoothness of the time- $t$  map  $\mathcal{P}^t$ , and of  $\rho$ , which gives the expression (8). The characterization (9) of the pseudo-stable manifold follows from general expressions in [35] and [36] after we set  $a$  as in (15).  $\square$

Note that theorem 1 limits the degree of smoothness of the manifolds  $W^{ps}(0)$  and  $W^{pu}(0)$  to the integer part of the eigenvalue ratio  $\lambda_1/\lambda_2$ , no matter how smooth the full Hamiltonian  $H$  is. This is not merely a technical limitation of our proof: most pseudo-hyperbolic invariant manifolds are less smooth than the underlying dynamical system.

To see this loss of smoothness in a simple example, consider the linear dynamical system  $\dot{x} = \lambda_2 x, \dot{y} = \lambda_1 y$  with  $\lambda_1 > \lambda_2$ . (In this model example, the single weakly unstable  $x$  direction replaces all centre-, stable and unstable directions in the more general setting of theorem 1). This two-dimensional model system has infinitely many pseudo-stable manifolds that are all tangent to the  $y = 0$  axis at the origin. Each such manifold can be written in the form  $y = Cx^{\lambda_1/\lambda_2}$  for some real constant  $C$ . Observe that unless  $C = 0$ , the maximum degree of differentiability for any pseudo-stable manifold at the origin is just  $\text{Int}[\lambda_1/\lambda_2]$ , even though the underlying linear dynamical system is arbitrarily many times differentiable.

Based on the above result, under conditions (2) and (8), codimension one pseudo-stable and pseudo-unstable invariant manifolds exist at the origin of the phase space. They intersect any nearby energy surface

$$\tilde{\mathcal{E}}_h = \{(p, q) \in \mathbb{R}^{2n} : H(p, q) = h > 0\}$$

transversely in the isoenergetic surfaces

$$W_h^{ps} = W^{ps}(0) \cap \tilde{\mathcal{E}}_h, \quad W_h^{pu} = W^{pu}(0) \cap \tilde{\mathcal{E}}_h,$$

which are codimension one within  $\tilde{\mathcal{E}}_h$ .

For any  $h > 0$  small enough, the intersection

$$\tilde{C}_h = W_h^{ps} \cap W_h^{pu}$$

is a smooth continuation of the surface  $C_h$  defined in (5). This is the case because  $W_h^{ps}$  and  $W_h^{pu}$  are smooth perturbations of  $E_{\lambda_2}^s$  and  $E_{\lambda_2}^u$  near the origin, and the latter two surfaces intersect transversely; hence their intersection smoothly perturbs under small enough perturbations. We conclude that  $\tilde{C}_h$  is diffeomorphic to near-critical energy surfaces of an  $(n - 1)$  degrees of freedom Hamiltonian with a rank- $(m - 1)$  saddle. We sketch the geometry of  $\tilde{C}$  and  $\tilde{C}_h$  in figure 7.

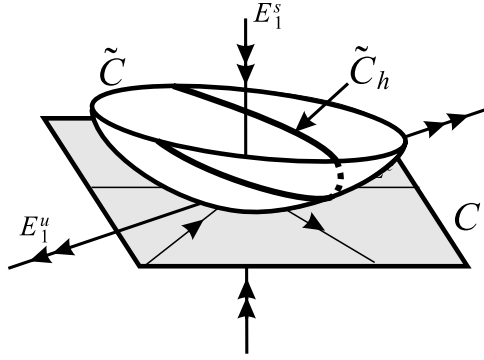


**Figure 7.** The manifold  $C$  deforms into  $\tilde{C}$  under the addition of higher-order terms to the quadratic Hamiltonian  $H_2$ . The intersection of  $\tilde{C}$  with the energy surface  $\mathcal{E}_h$  is denoted by  $\tilde{C}_h$ .

We note that  $\tilde{C}_h$  is an  $\bar{r}$  times continuously differentiable manifold, as it is the transverse intersection of two manifolds of the same degree of smoothness. Since the Hamiltonian  $H$  is of class  $\mathcal{C}^r$  for any positive  $r$ , the real limitation on  $\bar{r}$  is the ratio of the two Lyapunov exponents,  $\lambda_1$  and  $\lambda_2$ . A Taylor expansion for  $\tilde{C}_h$  near the origin is only guaranteed to exist up to order  $\bar{r}$ .

The stable manifold of  $\tilde{C}_h$  is given by

$$W^s(\tilde{C}_h) = W_h^{ps},$$

a codimension one surface within the energy surface  $\tilde{\mathcal{E}}_h$ . Similarly, the unstable manifold of  $\tilde{C}_h$ ,

$$W^u(\tilde{C}_h) = W_h^{pu},$$

is a codimension one surface within  $\tilde{\mathcal{E}}_h$ .

The manifolds  $W^s(\tilde{C}_h)$  and  $W^u(\tilde{C}_h)$  will be small deformations of their linearized counterparts,  $W^s(C_h)$  and  $W^u(C_h)$  (see (5)). In analogy with their linear counterparts,  $W^s(\tilde{C}_h)$  and  $W^u(\tilde{C}_h)$  can be partitioned into two parts: a forward part and a backward part, which satisfy

$$W_f^s(\tilde{C}_h) = \left\{ (p, q) \in \mathbb{R}^{2n} : \frac{1}{2} \sum_{i=2}^m (p_i^2 - \lambda_i^2 q_i^2) + \frac{1}{2} \sum_{i=m+1}^n (p_i^2 + \omega_i^2 q_i^2) \right. \\ \left. + f(0, p_2, \dots, p_n, q_2, \dots, q_n) = h > 0, p_1 = -\lambda_1 q_1 \geq 0 \right\},$$

$$W_b^s(\tilde{C}_h) = \left\{ (p, q) \in \mathbb{R}^{2n} : \frac{1}{2} \sum_{i=2}^m (p_i^2 - \lambda_i^2 q_i^2) + \frac{1}{2} \sum_{i=m+1}^n (p_i^2 + \omega_i^2 q_i^2) \right. \\ \left. + f(0, p_2, \dots, p_n, q_2, \dots, q_n) = h > 0, p_1 = \lambda_1 q_1 \geq 0 \right\},$$

$$W_f^u(\tilde{C}_h) = \left\{ (p, q) \in \mathbb{R}^{2n} : \frac{1}{2} \sum_{i=2}^m (p_i^2 - \lambda_i^2 q_i^2) + \frac{1}{2} \sum_{i=m+1}^n (p_i^2 + \omega_i^2 q_i^2) \right. \\ \left. + f(0, p_2, \dots, p_n, q_2, \dots, q_n) = h > 0, p_1 = -\lambda_1 q_1 \leq 0 \right\},$$

$$W_b^u(\tilde{C}_h) = \left\{ (p, q) \in \mathbb{R}^{2n} : \frac{1}{2} \sum_{i=2}^m (p_i^2 - \lambda_i^2 q_i^2) + \frac{1}{2} \sum_{i=m+1}^n (p_i^2 + \omega_i^2 q_i^2) \right. \\ \left. + f(0, p_2, \dots, p_n, q_2, \dots, q_n) = h > 0, p_1 = \lambda_1 q_1 \leq 0 \right\}.$$

The forward and backward parts of these two manifolds

$$W_f(\tilde{C}_h) = W_f^s(\tilde{C}_h) \cup W_f^u(\tilde{C}_h), \quad W_b(\tilde{C}_h) = W_b^s(\tilde{C}_h) \cup W_b^u(\tilde{C}_h)$$

join to yield two  $(2n - 2)$ -dimensional invariant tubes that, respectively, correspond to the forward and backward reactive tubes [26–33]. They are embedded in the  $(2n - 1)$ -dimensional energy shell and hence are codimension one. Consequently, the states within these tubes remain confined to the tubes and flow from the interior of  $W_j^s$  into the interior of  $W_j^u$  (where  $j = f$  or  $b$ ) [2].

We define two transition states as cross-section surfaces in each of the forward and backward reactive tubes,

$$\text{TS}_f(\tilde{C}_h) = \left\{ (p, q) \in \mathbb{R}^{2n} : \frac{1}{2} p_1^2 + \frac{1}{2} \sum_{i=2}^m (p_i^2 - \lambda_i^2 q_i^2) + \frac{1}{2} \sum_{i=m+1}^n (p_i^2 + \omega_i^2 q_i^2) \right. \\ \left. + f(I_1, p_2, \dots, p_n, q_2, \dots, q_n) = h > 0, q_1 = 0, p_1 \geq 0 \right\},$$

$$\text{TS}_b(\tilde{C}_h) = \left\{ (p, q) \in \mathbb{R}^{2n} : \frac{1}{2} p_1^2 + \frac{1}{2} \sum_{i=2}^m (p_i^2 - \lambda_i^2 q_i^2) + \frac{1}{2} \sum_{i=m+1}^n (p_i^2 + \omega_i^2 q_i^2) \right. \\ \left. + f(I_1, p_2, \dots, p_n, q_2, \dots, q_n) = h > 0, q_1 = 0, p_1 \leq 0 \right\},$$

the forward and backward transition states. Their union is a  $(2n - 2)$ -dimensional unbounded surface and their intersection is simply the pseudo-NHIM,  $\tilde{C}_h$ . And finally, we observe that all states exterior to the two reactive tubes do not react, that is, they are confined to either reactant or product regions of phase space for all time.

The main differences between  $W^s(\tilde{C}_h)$  and the stable manifold of a pseudo-NHIM in the rank-one saddle case are:

- The manifold  $W^s(\tilde{C}_h)$  is constructed as a pseudo-stable manifold, and hence it is non-unique. However, it is tangent to the unique pseudo-stable subspace,  $E_{\lambda_2}^s$ , and hence its Taylor expansion is unique to order  $\bar{r}$ .
- The manifold  $W^s(\tilde{C}_h)$  is guaranteed to be of class  $\mathcal{C}^{\bar{r}}$ .
- Typical solutions in  $W^s(\tilde{C}_h)$  do not tend to  $\tilde{C}_h$  in forward time, but cannot leave  $\tilde{C}_h$  at rates faster than  $\exp [t (\lambda_2 + \lambda_1 / \text{Int} [\lambda_1 / \lambda_2]) / 2]$  while near  $\tilde{C}_h$ .

Similar comments can be made for  $W^u(\tilde{C}_h)$ .

#### 4. Application: two-electron atoms

When higher-dimensional saddles with more than one unstable direction are present it is only natural for the multiple unstable directions to compete with each other during the passage through this saddle and for one direction to dominate over the others depending on the relative

values of the Lyapunov coefficients [39]. A prominent example of such behaviour comes from atomic physics, and specifically from the threshold ionization behaviour of highly excited two-electron atoms like helium [40]. This phenomenon was first described by Wannier [41] in the context of his famous threshold law: simply stated, if one assumes that the electrons (denoted as  $e$ ) and the nucleus (denoted as  $Z$ ) are in the linear configuration  $eZe$ , then double ionization has to take place by both of the electrons moving away from the nucleus totally symmetrically; the slightest asymmetry in their dynamics will cause one of the electrons to fall towards the nucleus and the other one to move away from it. So, not surprisingly, correlated double ionization is much more difficult to arrange than its alternatives, and will, in an ensemble of many random initial conditions and configurations, be washed out by the antisymmetric electron exchange.

In our recent investigation of helium ionization in external fields [39], we found precisely this connection, namely that of the two unstable directions that the rank-two saddle (the Stark saddle) supports, the totally symmetric one (leading to non-sequential, correlated double ionization) is slower than the antisymmetric one, which leads to the exchange of electrons. This finding also explains why classically, for arbitrary initial configurations, in a symmetrically excited helium atom usually one electron moves towards the nucleus while the other moves away. The relative rates of crossing the associated barriers are of course related to the Lyapunov exponents. As the rate of the antisymmetric process is greater than that of the symmetric mode, the antisymmetric mode dominates.

More generally, the scattering of electrons from ions in the presence of fields, especially time-dependent ones, is finding many applications in laser–matter interaction physics today [25]. The correlated double ionization of helium in the presence of an intense laser field has served up a big surprise to physicists: In strong contrast to the static-field scenario, the non-sequential, correlated double ionization rates are found to be several orders of magnitude greater than the uncorrelated mechanism allows, making this phenomenon one of the most dramatic manifestations of electron–electron correlation in nature [42–59]. The precise mechanism that makes correlation so effective is far from settled and subject to intensive research, both experimental and theoretical. Thus far, the so-called re-collision (or three-step) scenario [43, 44], in which the ionized electron is hurled back at the ion after absorbing a lot of energy from the laser field and dislodges the core electron, seems in best accord with experiments. Moreover, many of the important features can be understood classically [25].

The re-collision scenario combines electron–ion scattering with the passage through the rank-two Stark saddle [49, 60, 61] and therefore offers a huge arena for fundamental research. The effect of time-dependent external fields is outside the scope of this work, but we are confident that the research on the effect of static fields detailed below will be a useful stepping stone in that direction.

#### 4.1. The model

The simplest system which ionizes non-sequentially is a helium atom in a static electric field [49, 60, 61]. This is a three-body problem. The three particles are the nucleus and two electrons. The mass of the nucleus is taken to be infinite. This is a simplification of the problem that is easily remedied if needed without affecting the results presented here. Atomic units are used, thus the mass of the electrons are taken to be unity. All energies are given in hartrees. The charge of the nucleus is +2 while the electrons have charge  $-1$ . This system has six degrees of freedom. The three degrees of freedom associated with the centre of mass are neglected as a direct result of the assumption of the nucleus having infinite mass. The six degrees of freedom describe the two vectors that point from the nucleus to each of the two electrons. This is illustrated in figure 8. The  $z$ -axis is defined to be in the direction

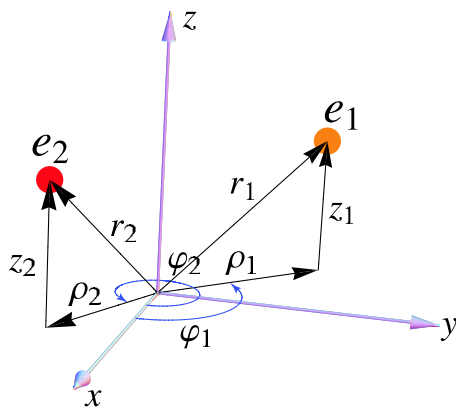


**Figure 8.** The physical coordinates. The physical variables are chosen to be the cylindrical coordinates and corresponding momenta of each of the electrons.

of the electric field. Each of the vectors describing the positions of the two electrons are represented in cylindrical coordinates,  $(\rho_1, \varphi_1, z_1)$  and  $(\rho_2, \varphi_2, z_2)$ . An additional integral of the motion exists, namely the angular momentum about the  $z$ -axis defined by the electric field. Consequently, the problem can be reduced to one of five degrees of freedom, which is standard for the  $n$ -body problem in a static electric field, see [37, 38].

The presence of the electric field gives rise to a Stark barrier. To ionize classically the electrons must escape over this barrier (quantum-mechanically they can also ionize by tunnelling under the barrier). If the external electric field is taken to be constant the Hamiltonian system defining the problem is autonomous. The Stark barrier gives rise to a fixed point in the ten-dimensional phase space associated with the five degrees of freedom. This fixed point is a rank-two saddle. In other words, it has three stable or elliptic directions (central directions) and two unstable or hyperbolic directions. One of the unstable directions is associated with the non-sequential (or correlated) ionization ( $\text{He} \rightarrow \text{He}^{2+} + 2e^-$ ) while the second unstable direction is associated with the non-sequential (or correlated) exchange ( $\text{He}^+ + e^-(A) \rightarrow \text{He}^+ + e^-(B)$ ) of electrons.

The initial Hamiltonian is given by

$$\begin{aligned}
 H = & \frac{1}{2} \left( P_{\rho_1}^2 + \frac{P_{\varphi_1}^2}{\rho_1^2} + P_{z_1}^2 \right) + \frac{1}{2} \left( P_{\rho_2}^2 + \frac{P_{\varphi_2}^2}{\rho_2^2} + P_{z_2}^2 \right) - \mathcal{F}(z_1 + z_2) - \frac{2}{\sqrt{\rho_1^2 + z_1^2}} - \frac{2}{\sqrt{\rho_2^2 + z_2^2}} \\
 & + \frac{1}{\sqrt{\rho_1^2 + \rho_2^2 - 2\rho_1\rho_2 \cos(\varphi_1 - \varphi_2) + (z_1 - z_2)^2}}. \tag{16}
 \end{aligned}$$

The first two terms are the kinetic energy of the two electrons. The third term represents the interaction of the two electrons with the electric field. Here the scalar  $\mathcal{F}$  represents the strength of the electric field. The fourth and fifth terms are the attractive interactions between the nucleus and the two electrons and the last term is the repulsive interaction between the two electrons. This Hamiltonian accounts for the motions of the electrons with respect to the nucleus.

The Hamiltonian (16) has six degrees of freedom. One of these can be eliminated by making use of the existence of the additional constant of the motion: the projection of the angular momentum on the  $z$ -axis. To achieve this we introduce a new set of coordinates

defined by the following linear canonical transformation  $\mathcal{G}$ :

$$\begin{aligned}
r &= (\rho_1 - \rho_2)/2 & R &= (\rho_1 + \rho_2)/2 \\
\varphi &= \varphi_1 - \varphi_2 & \Phi &= \varphi_1 + \varphi_2 \\
z &= (z_1 - z_2)/2 & Z &= (z_1 + z_2)/2 \\
P_r &= P_{\rho_1} - P_{\rho_2} & P_R &= P_{\rho_1} + P_{\rho_2} \\
P_\varphi &= (P_{\varphi_1} - P_{\varphi_2})/2 & P_\Phi &= (P_{\varphi_1} + P_{\varphi_2})/2 \\
P_z &= P_{z_1} - P_{z_2} & P_Z &= P_{z_1} + P_{z_2}.
\end{aligned} \tag{17}$$

The transformed Hamiltonian is given by

$$\begin{aligned}
H &= \frac{P_r^2 + P_R^2}{4} + \frac{P_z^2 + P_Z^2}{4} + \frac{(P_\varphi + P_\Phi)^2}{2(r+R)^2} + \frac{(P_\varphi - P_\Phi)^2}{2(r-R)^2} - 2\mathcal{F}Z - \frac{2}{\sqrt{(r+R)^2 + (z+Z)^2}} \\
&\quad - \frac{2}{\sqrt{(r-R)^2 + (z-Z)^2}} + \frac{1}{2\sqrt{r^2 \cos^2(\varphi/2) + R^2 \sin^2(\varphi/2) + z^2}}.
\end{aligned} \tag{18}$$

It is evident that  $H$  is independent of  $\Phi$ , therefore  $P_\Phi$  is an integral of the motion and can be taken to be a parameter. In this manner the Hamiltonian (18) is reduced to one having five degrees of freedom.

*4.1.1. The fixed point.* The fixed point of the Hamiltonian vector field is readily obtained by setting the right-hand side of Hamilton's equations of motion equal to zero: first note that the vector field only has a fixed point provided that  $P_\Phi = 0$ . Next observe that since the Hamiltonian is a sum of the kinetic and potential energies, all of the momenta must also equal zero,  $P_r = P_R = P_\varphi = P_z = P_Z = 0$ . And finally, assuming  $\mathcal{F} > 0$ , the location of the fixed point is given by  $r = z = 0$ ,  $\varphi = \pi$ ,  $R = R_s = r_s/2 = 3^{1/4}/(2\sqrt{\mathcal{F}})$  and  $Z = Z_s = \sqrt{3}r_s/2 = 3^{3/4}/(2\sqrt{\mathcal{F}})$ , where  $r_s = \sqrt{\sqrt{3}/\mathcal{F}}$ . The energy of the fixed point is  $H_0 = -6/r_s = -6\sqrt{\mathcal{F}/\sqrt{3}}$ . Also note that symmetry of the stationary configuration is characterized by the  $C_{2v}$  point group.

#### 4.2. The normal modes

The normal modes are defined by the dynamics in the immediate vicinity of the saddle point. To investigate these dynamics one first shifts the origin to the saddle point and then expands the Hamiltonian in a Taylor series about the saddle point. The constant term gives the energy of the saddle point and the linear term is identically equal to zero as the origin is a fixed point. The quadratic term is used to define the normal mode variables by requiring that it takes the form

$$\begin{aligned}
H_2 &= \frac{1}{2}(P_U^2 - \lambda_U^2 U^2) \quad (A_1, \text{unstable}, \lambda_U^2 = (\sqrt{19} - 1)/r_s^3) \\
&\quad + \frac{1}{2}(P_u^2 - \lambda_u^2 u^2) \quad (B_2, \text{unstable}, \lambda_u^2 = (\sqrt{13} + 2)/r_s^3) \\
&\quad + \frac{1}{2}(P_V^2 + \omega_V^2 V^2) \quad (A_1, \text{stable}, \omega_V^2 = (\sqrt{19} + 1)/r_s^3) \\
&\quad + \frac{1}{2}(P_v^2 + \omega_v^2 v^2) \quad (B_2, \text{stable}, \omega_v^2 = (\sqrt{13} - 2)/r_s^3) \\
&\quad + \frac{1}{2}(P_\phi^2 + \omega_\phi^2 \phi^2) \quad (B_1, \text{stable}, \omega_\phi^2 = 2/r_s^3).
\end{aligned} \tag{19}$$

Observe that the first two terms correspond to parabolic barriers and the last three terms correspond to harmonic oscillators.

**Table 1.** The normal mode frequencies. Shown here are the stabilities, symmetry properties and frequencies of the five normal modes. Note that the frequencies of the unstable modes are imaginary and that the point group of the stationary configuration is  $C_{2v}$ .

Mode	Stability	Irreducible representation	Frequency
$U$	Unstable	$A_1$	$1.21389i \mathcal{F}^{3/4}$
$V$	Stable	$A_1$	$1.53327 \mathcal{F}^{3/4}$
$u$	Unstable	$B_2$	$1.56815i \mathcal{F}^{3/4}$
$v$	Stable	$B_2$	$0.839251 \mathcal{F}^{3/4}$
$\phi$	Stable	$B_1$	$0.936687 \mathcal{F}^{3/4}$

Methods for the construction of transformations to normal mode variables are well known [37, 38, 62]. The transformation, which we denoted as  $\mathcal{R}$ , is given by

$$\begin{aligned}
 R &= R_s + (U \cos \alpha - V \sin \alpha)/\sqrt{2} & P_R &= \sqrt{2}(P_U \cos \alpha - P_V \sin \alpha) \\
 Z &= Z_s + (U \sin \alpha - V \cos \alpha)/\sqrt{2} & P_Z &= \sqrt{2}(P_U \sin \alpha + P_V \cos \alpha) \\
 r &= (u \cos \beta - v \sin \beta)/\sqrt{2} & P_r &= \sqrt{2}(P_u \cos \beta - P_v \sin \beta) \\
 z &= (u \sin \beta + v \cos \beta)/\sqrt{2} & P_z &= \sqrt{2}(P_u \sin \beta + P_v \cos \beta) \\
 \phi &= (2\sqrt{2}/r_s)\phi + \pi, & P_\phi &= (r_s/(2\sqrt{2}))P_\phi,
 \end{aligned} \tag{20}$$

where  $\alpha = \frac{\pi}{2} - \frac{1}{2} \arctan \left[ 3\sqrt{3}/7 \right]$  and  $\beta = \frac{\pi}{2} - \frac{1}{2} \arctan \left[ 3\sqrt{3}/5 \right]$ .

A straightforward group-theoretical analysis [63] identifies the symmetry properties of the normal modes. The point group of the saddle point configuration is  $C_{2v}$ . The irreducible representations of the five normal modes are  $\Gamma = 2A_1 + B_1 + 2B_2$ . The symmetry properties and frequencies of the normal modes are given in table 1.

It is easy to obtain the higher-order terms of the Hamiltonian, i.e. the terms  $H_3, H_4, \dots$ , in normal mode variables.

### 4.3. The normal form

Standard methods pioneered by Deprit [64] are used to transform the Hamiltonian into normal form. The first step in this process is to transform the quadratic terms of the Hamiltonian into normal form. Once the canonical transformation that takes the quadratic terms into normal form is known, the cubic and higher-order terms of the Hamiltonian are transformed into these variables. It should be noted that at this stage the higher-order terms are not yet in normal form. Transforming these higher-order terms into normal form is accomplished by a sequence of Lie–Deprit transformations [38]. While in principle this is a straightforward process, in practice the transformation of the higher-order terms is not trivial and requires the use of computers.

**4.3.1. The quadratic terms.** For rank-two saddles the normal form for the quadratic term of the Hamiltonian is

$$H_2 = \lambda_1 P_1 Q_1 + \lambda_2 P_2 Q_2 + i \omega_3 P_3 Q_3 + i \omega_4 P_4 Q_4 + i \omega_5 P_5 Q_5. \tag{21}$$

Note that the first two terms are the unstable modes while the final three modes are stable. The transformation, denoted  $\mathcal{D}$ , of the quadratic term of the Hamiltonian from the normal mode

variables (19) into the normal form (21) is well known,

$$\begin{aligned}
 U &= \sqrt{\frac{1}{2\lambda_2}}(P_2 - Q_2) & P_U &= \sqrt{\frac{\lambda_2}{2}}(P_2 + Q_2), \\
 V &= \iota \sqrt{\frac{1}{2\omega_3}}(P_3 - \iota Q_3) & P_V &= \sqrt{\frac{\omega_3}{2}}(P_3 + \iota Q_3), \\
 u &= \sqrt{\frac{1}{2\lambda_1}}(P_1 - Q_1) & P_u &= \sqrt{\frac{\lambda_1}{2}}(P_1 + Q_1), \\
 v &= \iota \sqrt{\frac{1}{2\omega_4}}(P_4 - \iota Q_4) & P_v &= \sqrt{\frac{\omega_4}{2}}(P_4 + \iota Q_4), \\
 \phi &= \iota \sqrt{\frac{1}{2\omega_5}}(P_5 - \iota Q_5) & P_\phi &= \sqrt{\frac{\omega_5}{2}}(P_5 + \iota Q_5),
 \end{aligned} \tag{22}$$

where  $\lambda_1 = \lambda_u > \lambda_2 = \lambda_U > 0$ , and  $\omega_3 = \omega_V > 0$ ,  $\omega_4 = \omega_v > 0$ ,  $\omega_5 = \omega_\phi > 0$ . Several observations are critical at this juncture. First note that the ratio of  $\lambda_1/\lambda_2 = (\sqrt{13} + 2)/(\sqrt{19} - 1)$  is irrational and independent of the strength of the electric field  $\mathcal{F}$ . Additionally, the ratios of the three frequencies are also irrational and independent of the field strength,  $\omega_3/\omega_5 = (\sqrt{19} + 1)/2$ ,  $\omega_4/\omega_5 = (\sqrt{13} - 2)/2$  and  $\omega_3/\omega_4 = (\sqrt{19} + 1)/(\sqrt{13} - 2)$ . This is important as it indicates that small divisors should not be an issue. Secondly, note that the modes have been ordered so as to satisfy (2). And finally note that, if the higher-order terms in the Hamiltonian are truncated, then the five quantities  $P_1, Q_1, P_2, Q_2, \iota P_3, Q_3, \iota P_4, Q_4$  and  $\iota P_5, Q_5$  are integrals of the motion.

**4.3.2. Higher-order terms.** The purpose of transforming the higher-order terms of the Hamiltonian into normal form is to obtain expressions for these terms as a function of the five invariants identified in the previous subsection. This is accomplished by a sequence of  $(N - 2)$  Lie–Deprit transformations [2, 3]. The result will be a Hamiltonian that is in normal form up to and including terms of the  $N$ th degree. If the Hamiltonian  $H$  is truncated at this level, the resulting Hamiltonian  $K$  is integrable. This is due to the fact that the frequencies  $\lambda_i$  and  $\omega_i$ 's are incommensurate. We use Deprit's method [64] to construct these transformation.

Each of the  $(N - 2)$  Lie–Deprit transformations transforms the next level of the Hamiltonian into normal form. Thus, the first transformation changes the cubic term of the Hamiltonian  $H_3$  into normal form, the second transforms the quartic term  $H_4$  into normal form, etc. We denote the entire series of transformations as  $\mathcal{NF}$ .

Consider the  $j$ th transformation. Each transformation involves two parts. In the first part the normal form of the  $(j + 2)$ th-degree term (i.e. the  $j$ th order term) of the Hamiltonian  $K_{j+2}$  and the associated generating function  $\mathcal{W}_{j+2}$  are constructed. In the second part the generating function  $\mathcal{W}_{j+2}$  is used to construct the transformation equations:  $P = P(P^\dagger, Q^\dagger)$  and  $Q = Q(P^\dagger, Q^\dagger)$  where  $P^\dagger$  and  $Q^\dagger$  are the transformed variables. In addition, the higher-order terms in the Hamiltonian are transformed into the new variables. Observe that both  $K_{j+2}$  and  $\mathcal{W}_{j+2}$  are sums of monomials of degree  $(j + 2)$  in the phase space variables.

The construction of the normal form of the  $(j + 2)$ th-degree term of the Hamiltonian is straightforward. This is due to the fact that the quadratic term of the Hamiltonian  $H_2$  has already been transformed into normal form (21). As a consequence, the Lie operator defined by this normal form will transform a monomial of a given degree into another monomial of the same degree. Thus, when the Lie operator acts on either a term of the Hamiltonian or the generating function, it returns a function that is of the same degree. As a consequence, it is

**Table 2.** Number of monomials in the phase space variables  $P_k^\dagger$ 's,  $Q_k^\dagger$ 's of the normal-form Hamiltonians  $K = \sum_{j=2}^{12} K_j/(j-2)!$  and of the generating functions  $\mathcal{W} = \sum_{j=3}^{12} \mathcal{W}_j/(j-3)!$  to order ten. The coefficients of these monomials are presented in the supplementary data (available at [stacks.iop.org/Non/24/527](https://stacks.iop.org/Non/24/527)).

Order	0	1	2	3	4	5	6	7	8	9	10
$K$	5	0	15	0	35	0	70	0	126	0	210
$\mathcal{W}$		72	220	596	1450	3232	6768	13304	25052	45008	78296

easy to split the intermediate Hamiltonians into the terms that belong to the kernel of the Lie operator, e.g. the monomials that are kept in the normal-form Hamiltonian and the terms that belong to the image of the Lie operator and must be incorporated to the generating function, after being multiplied by an appropriate constant, see the details in [65].

After the Hamiltonian is transformed into normal form to a given degree the higher-order terms are truncated. The resulting Hamiltonian  $K$  is integrable. This is a consequence of the real and imaginary frequencies being incommensurate. As a direct consequence the two reactive modes associated with the two hyperbolic degrees of freedom decouple. Similarly, the three elliptic modes associated with the centre manifold also decouple. Furthermore the quantities  $P_k^\dagger Q_k^\dagger$  for  $k = 1, \dots, 5$  are integrals of the motion of the dynamical system defined by  $K$ . The action variables  $I_i$  are given by  $I_1 = P_1^\dagger Q_1^\dagger$ ,  $I_2 = P_2^\dagger Q_2^\dagger$ ,  $I_3 = \iota P_3^\dagger Q_3^\dagger$ ,  $I_4 = \iota P_4^\dagger Q_4^\dagger$  and  $I_5 = \iota P_5^\dagger Q_5^\dagger$ , Hamiltonian  $K$  reads as

$$K(I_1, I_2, I_3, I_4, I_5) = \sum_{n=2}^N K_n(I_1, I_2, I_3, I_4, I_5) \quad (23)$$

with

$$K_n(I_1, I_2, I_3, I_4, I_5) = \sum_{i+j+k+l+m=n/2} a_{ijklm} I_1^i I_2^j I_3^k I_4^l I_5^m$$

where the sum is over all  $i, j, k, l$  and  $m$  such that  $i + j + k + l + m = n/2$ . Also note that if  $n$  is odd, then  $K_n = 0$ . The three constants of the motion,  $I_3, I_4$  and  $I_5$  are the classical action variables associated with the three non-reactive degrees of freedom. The integrals  $I_1$  and  $I_2$  are associated with the reactive coordinates. The coefficients,  $a_{ijklm}$ , are to be obtained via a normal-form construction.

**4.3.3. Transformation to 10th order.** While that the construction of the Lie–Deprit transform is conceptually simple, the size of the calculations requires the use of computers. The difficulty is immediately apparent when one considers the number of terms contained in each of the terms in the Hamiltonian and the generating function. The number of terms of  $H$  and  $\mathcal{W}$  are given in table 2.

The normal form of the Hamiltonian given in (16) to 10th order (that is, to degree  $N = 12$ ) was obtained with an electric field strength given by  $\mathcal{F} = 0.137$ . The 0th, 2nd, 4th and 6th degree coefficients  $a_{ijklm}$  defined in (23) are given in table 3. The Hamiltonian and the generating function to 10th order ( $N = 12$ ) are given in the supplementary data (available at [stacks.iop.org/Non/24/527](https://stacks.iop.org/Non/24/527)). Note that the monomial  $a_{00000}$  is a constant term equal to the energy  $H_0$  of the fixed point.

The occurrence of small divisors in the denominators of the monomials forming the generating functions is possible. Even when this can occur for particular combinations of the frequencies, we have not observed behaviour of this nature. We discuss this next.

**Table 3.** Coefficients for the 0th, 2nd, 4th and 6th degree terms in the normal-form Hamiltonian. Terms of odd degree are identically equal to zero. The higher-degree terms can be found in the supplementary data (available at [stacks.iop.org/Non/24/527](http://stacks.iop.org/Non/24/527)).

$a_{00000}$	-1.687 451 192 67		
$a_{10000}$	0.353 125 532 133	$a_{01000}$	0.273 349 588 055
$a_{00100}$	0.345 269 120 501	$a_{00010}$	0.188 987 049 505
$a_{00001}$	0.210 928 348 692		
$a_{20000}$	0.020 105 729 600 9	$a_{11000}$	0.013 190 467 283 3
$a_{02000}$	0.006 349 431 444 84	$a_{10100}$	0.060 858 000 660 6
$a_{01100}$	0.000 094 753 810 357 3	$a_{00200}$	0.023 170 420 249 6
$a_{10010}$	0.004 517 654 827 51	$a_{01010}$	-0.001 072 908 520 62
$a_{00110}$	0.0079 424 987 096 1	$a_{00020}$	0.003 686 841 487 45
$a_{10001}$	0.008 790 443 952 04	$a_{01001}$	-0.000 331 815 657 835
$a_{00101}$	0.026 313 927 435 3	$a_{00011}$	0.148 845 254 292
$a_{00002}$	0.006 920 986 351 91		
$a_{30000}$	0.000 152 170 579 737	$a_{21000}$	-0.003 184 944 571 42
$a_{12000}$	0.000 508 958 521 844	$a_{03000}$	0.000 330 681 134 588
$a_{20100}$	0.004 621 933 901 59	$a_{11100}$	-0.008 814 229 637 32
$a_{02100}$	-0.000 584 305 387 516	$a_{10200}$	0.002 839 597 094 90
$a_{01200}$	-0.001 294 136 207 96	$a_{00300}$	-0.000 630 993 650 544
$a_{20010}$	-0.000 572 340 996 592	$a_{11010}$	-0.001 443 414 920 42
$a_{02010}$	-0.000 488 826 934 323	$a_{10110}$	-0.004 934 441 776 54
$a_{01110}$	-0.002 114 817 985 54	$a_{00210}$	-0.004 859 672 108 43
$a_{10020}$	0.001 143 585 135 86	$a_{01020}$	-0.000 242 743 590 196
$a_{00120}$	0.002 166 490 287 42	$a_{00030}$	0.000 150 191 479 323
$a_{20001}$	0.004 195 821 643 95	$a_{11001}$	-0.001 537 470 241 27
$a_{02001}$	-0.000 468 867 739 930	$a_{10101}$	-0.001 903 202 659 67
$a_{01101}$	-0.002 110 357 355 99	$a_{00201}$	0.003 428 040 946 51
$a_{10011}$	-0.055 593 544 668 3	$a_{01011}$	-0.003 157 146 413 92
$a_{00111}$	0.077 571 413 495 9	$a_{00021}$	-0.428 516 226 894
$a_{10002}$	0.003 577 541 199 08	$a_{01002}$	-0.000 635 133 922 605
$a_{00102}$	0.004 669 795 919 56	$a_{00012}$	0.462 244 626 534
$a_{00003}$	0.000 970 880 875 134		

**4.3.4. Error estimates for the normal form.** Truncating the higher-order terms of the normal form introduces an error. The typical method of estimating the size of this error is to compute the upper bounds for the remainder terms that are to be truncated. This procedure is laborious and often the bounds obtained are not sharp enough.

An alternative procedure is followed here. Instead of seeking the bounds for the monomials appearing in the remainder, we identify the neighbourhood of the fixed point in which the error introduced in the truncation process is sufficiently small. This is achieved using two different techniques.

- (i) Consider the five integrals of motion  $I_k$  for  $k = 1, \dots, 5$  of the truncated normal-form Hamiltonian  $K$ . These integrals commute with  $K$ , i.e.  $\{I_k, K\} = 0$  for  $k = 1, \dots, 5$ . The corresponding polynomials, which we denote  $I_k^*$  and are obtained from the  $I_k$ 's using the inverse Lie transformation, are not integrals of the full Hamiltonian. They do not commute with  $H$ ,  $\{I_k^*, H\} \neq 0$  for  $k = 1, \dots, 5$ . The goal is to define a volume (ball) in phase space surrounding the fixed point such that the quantities  $|\{I_k^*, H\}|/|H|$  evaluated within this ball have an upper bound that is sufficiently small.

To implement this idea a ball, in phase space, of radius  $1/10$  was defined. Then 100 random phase points within this ball were chosen and the value of the quantities  $|\{I_k^*, H\}|/|H|$  calculated for  $k = 1, \dots, 5$ . This yielded  $1.082795\dots \times 10^{-13}$  as an upper bound. The Poisson brackets are proportional to the rate at which the approximate integrals of the motion  $I_k^*$  vary with time.

These calculations were carried out in the variables defined by (17). The canonical transformation to these variables from the normal-form variables to the new set of variable (i.e. the variables  $P^\dagger$  and  $Q^\dagger$ ) is given by

$$T^{-1} = \mathcal{R}^{-1} \circ \mathcal{D}^{-1} \circ \mathcal{N}F^{-1}.$$

In these variables the actions are given by  $I_k = T^{-1}(P_k^\dagger, Q_k^\dagger)$ . The Hamiltonian in these variables is given in (18).

- (ii) Compare the Hamiltonian (18) with the Hamiltonian obtained by back transforming the normal-form Hamiltonian  $K$ . More concretely, calculate the Hamiltonian  $T^{-1}(K)$ . Then subtract the Taylor expansion to order 10 of (18)  $T^{-1}(K) - \sum_{j=2}^{12} H_j/(j-2)!$ . The result is zero. To avoid this, modify the Hamiltonian  $K$  slightly. Apply the inverse transformation to the modified normal-form Hamiltonian defined as  $\bar{K} = \sum_{j=2}^{12} \bar{K}_j/(j-2)!$  where  $\bar{K}_j = K_j$  for  $2 \leq j \leq 12$ ,  $\bar{K}_{11} = K_{11} + K_{12}/12$  and  $\bar{K}_{12} = 0$  and then subtract the Taylor expansion of (18) to obtain  $T^{-1}(\bar{K}) - \sum_{j=2}^{12} H_j/(j-2)!$ . Evaluate the expression  $|T^{-1}(\bar{K}) - H|/|H|$ . This error term is of the order of  $\mathcal{O}((P_k, Q_k)^{13})$ , i.e. it is of the form  $\mathcal{O}((P_k, Q_k)^{N+1})$  for an arbitrary  $N$ . Thus this quantity represents the first term of the global truncating error function.

As in the case of the first integrals, a sample of 1000 random phase points that lie within a nine-ball of radius  $1/10$  centred at the fixed point was chosen. Then the error term defined above was evaluated for these points. This yields an estimation of the relative error of the truncation procedure. The mean value for this error is  $3.841425\dots \times 10^{-9}$ .

Both checks indicate that, within nine-balls of radius  $1/10$  centred at the fixed points in phase space (ten-dimensional), reliable estimates of the relative error between Hamiltonians is of order of  $10^{-9}$  while the independent check of the approximate integrals of motion is of order  $10^{-13}$ . This implies that all the geometrical structures inside these balls, namely, the nonlinear continuation of the pseudo-NHIM, their stable and unstable manifolds and the transition states are all constructed with a global error of  $10^{-9}$  or less. Consequently, we are confident of our results within this tolerance.

**4.3.5. Theorem 1 revisited.** Theorem 1 addresses the existence of the pseudo-NHIM and its stable and unstable manifolds. It states a number of conditions and restrictions that must be satisfied. Central to these requirements are the two Lyapunov exponents,  $\lambda_1$  and  $\lambda_2$ . Their values are given in table 1. The ratio of these exponents is  $\lambda_1/\lambda_2 = (\sqrt{13} + 2)/(\sqrt{19} - 1) = 1.29184\dots$ . The theorem guarantees that the manifolds of interest are of at least class  $\mathcal{C}^{\bar{r}}$  where  $\bar{r}$  is the integer part of the ratio of the exponents  $\bar{r} = \text{Int}[\lambda_1/\lambda_2] = 1$ . Thus these surfaces are guaranteed to be at least of class  $\mathcal{C}^1$  in the neighbourhood of the rank-two saddle where the normal-form computations are valid.

If the condition  $e^{\lambda_2} < a < e^{\lambda_1/\rho}$  where  $\rho = \text{Int}[\lambda_1/\lambda_2] = 1$  and  $a = \exp[(\lambda_2 + \lambda_1/\text{Int}[\lambda_1/\lambda_2])/2]$  is satisfied then Irwin's theorem [35, 36] is applicable. Evaluating this inequality yields  $1.31435\dots < 1.36784\dots < 1.42350\dots$  thus theorem 1 is applicable in the present case.

In the exercise described above we constructed the manifolds of interest to 10th order (12th degree,  $N = 12$ ). As the theorem only guarantees that these manifold are of class

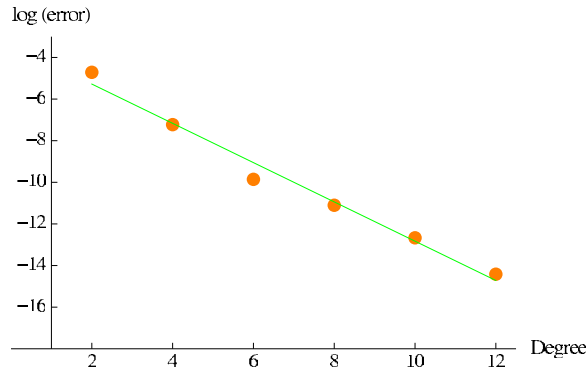


**Figure 9.** Logarithm of the estimate of the error in the integrals of the motion versus the degree to which the calculations were carried. The line is a linear fit to the data.

$\mathcal{C}^1$  one might have expected difficulties to occur. Nevertheless, the estimations of the tail of the normal-form transformations made in the previous subsection suggest the good behaviour of the approximations to the degree we have carried out the computations. The errors in the approximate integrals of motion and in the estimates based on the composition of the Hamiltonians decrease as we increase  $N$ . In figure 9 we plot the logarithm of the estimate of the error in the integrals versus the degree to which the calculations were carried. Here we have fixed a ball in phase space of size  $1/10$  centred at the rank-two saddle and take the maximum values of  $|\{I_k^*, H\}|/|H|$  for  $k = 1, \dots, 5$  for the different approximations  $I_k^*$  for different  $N$ 's. Note that  $I_k^*$  are polynomials of degree  $N$ . We see that this measure of the error appears to vary linearly with the order of the calculation.

As a conclusion, even when a high-order of smoothness of the manifolds cannot be guaranteed, the simulations show that the approximations of the geometrical structures through high-order normal forms are well behaved in the neighbourhood of the rank-two saddle.

#### 4.4. The dynamical implications

In addition to obtaining the transformed or normal-form Hamiltonian (23), the normalization algorithm also yields the transformation equations between the normal mode variables as defined in (19) (also see table 1) and the normal-form action-angle variables, that is,

$$\begin{aligned}
 U &= U(I_1, \dots, I_5, \theta_1, \dots, \theta_5) & P_U &= P_U(I_1, \dots, I_5, \theta_1, \dots, \theta_5), \\
 V &= V(I_1, \dots, I_5, \theta_1, \dots, \theta_5) & P_V &= P_V(I_1, \dots, I_5, \theta_1, \dots, \theta_5), \\
 u &= u(I_1, \dots, I_5, \theta_1, \dots, \theta_5) & P_u &= P_u(I_1, \dots, I_5, \theta_1, \dots, \theta_5), \\
 v &= v(I_1, \dots, I_5, \theta_1, \dots, \theta_5) & P_v &= P_v(I_1, \dots, I_5, \theta_1, \dots, \theta_5), \\
 \phi &= \phi(I_1, \dots, I_5, \theta_1, \dots, \theta_5) & P_\phi &= P_\phi(I_1, \dots, I_5, \theta_1, \dots, \theta_5).
 \end{aligned} \tag{24}$$

The normal-form Hamiltonian is integrable and we can immediately write down the time development of action-angle variables. The actions are constants of the motion and the angles develop linearly in time,

$$\begin{aligned}
 I_i(t) &= I_i(0), \\
 \theta_i(t) &= \nu_i t + \theta_i(0)
 \end{aligned} \tag{25}$$

for  $i = 1, \dots, 5$  and where the angular frequency is

$$\nu_i(I_1, \dots, I_5) = \frac{\partial K(I_1, \dots, I_5)}{\partial I_i}. \tag{26}$$

These expressions can be substituted directly into (24) giving the time development of the normal mode variables. Substituting these results into (20) and then into (17) yields the time development of the original physical variables.

In the subsections that follow we will use these results to examine the character of the dynamics confined to the various manifolds discussed above. In particular, we will examine the dynamics in both the normal mode and the original physical variables.

*4.4.1. The centre manifold and the NHIM.* The centre manifold of the rank-two saddle is a six-dimensional manifold embedded in the full ten-dimensional phase space. It is specified by setting the values of the action-angles variables associated with the two hyperbolic degrees of freedom equal to zero,

$$\begin{aligned} I_1 = 0 & \quad \theta_1 = 0, \\ I_2 = 0 & \quad \theta_2 = 0. \end{aligned} \tag{27}$$

The centre manifold is foliated by a three-parameter family of invariant three-tori. The parameters can be taken to be the action variables of the elliptic degrees of freedom ( $I_3, I_4, I_5$ ). The corresponding angle variables ( $\theta_3, \theta_4, \theta_5$ ) provide a coordinate system on each of the invariant tori.

Consider the action space defined by the three elliptic action variables. This space is a representation of the centre manifold. Every point in it corresponds to an invariant torus and is characterized by the value of the energy  $K(0, 0, I_3, I_4, I_5)$ . Specifying the value of the energy defines a two-dimensional surface in the three-dimensional elliptic action space. This surface is a representation of the NHIM. Each point in the surface corresponds to an invariant torus, which is embedded in the NHIM. The three corners of the NHIM, that is, the points where the NHIM intersects the three action axes correspond to periodic orbits. These orbits are fundamental dynamical modes of the NHIM. The orbits associated with these three fundamental modes are shown in figures 10 and 11. In the first figure the dynamics are shown in terms of the normal mode variables and in the second the same orbits are shown in the physical coordinate space. For these and all subsequent examples the energy is taken to be 0.025 hartrees above the barrier height.

In figure 10 we take advantage of the fact that normal modes decouple in the vicinity of the saddle point and plot the dynamics in the five two-dimensional phase spaces corresponding to each of the normal modes. Note that in each of these three examples the dynamics are confined to the origin of the two subspaces associated with the hyperbolic degrees of freedom. They satisfy (27) and consequently are confined to the NHIM. The differences between these three orbits are seen in the phase spaces associated with the stable or elliptic modes. The periodic orbit associated with the stable  $A_1$  mode is seen in figure 10(a). Here the values of the action variables in the  $B_1$  and  $B_2$  modes are equal to zero,  $I_4 = 0$  and  $I_5 = 0$ . Similarly, in figures 10(b) and 10(c) the periodic orbits associated with the stable  $B_2$  and  $B_1$  modes are shown. For the  $B_2$  mode  $I_3 = 0$  and  $I_5 = 0$ , and for the  $B_1$  mode  $I_3 = 0$  and  $I_4 = 0$ .

The orbits seen in figure 10 are shown in the physical coordinate space in figure 11. In figure 11(a) we see the stable  $A_1$  mode. A consequence of choosing  $\Phi = 0$  is that the dynamics are confined to the  $yz$ -plane. The fixed point corresponds to both electrons sitting at rest at the two dots. Note that as the two electrons cross above the saddle point their momenta are mirror images, and consequently, the two electrons are in phase as they traverse their own periodic orbits in the physical coordinate space. The  $B_2$  mode is also confined to the  $yz$ -plane. The coordinate space dynamics associated with this mode are shown in figure 11(b). Here, as the electrons cross above the saddle point, the momenta are not mirror images but rather inverted. The two electrons traverse symmetrical orbits but are out of phase with each other. And finally,

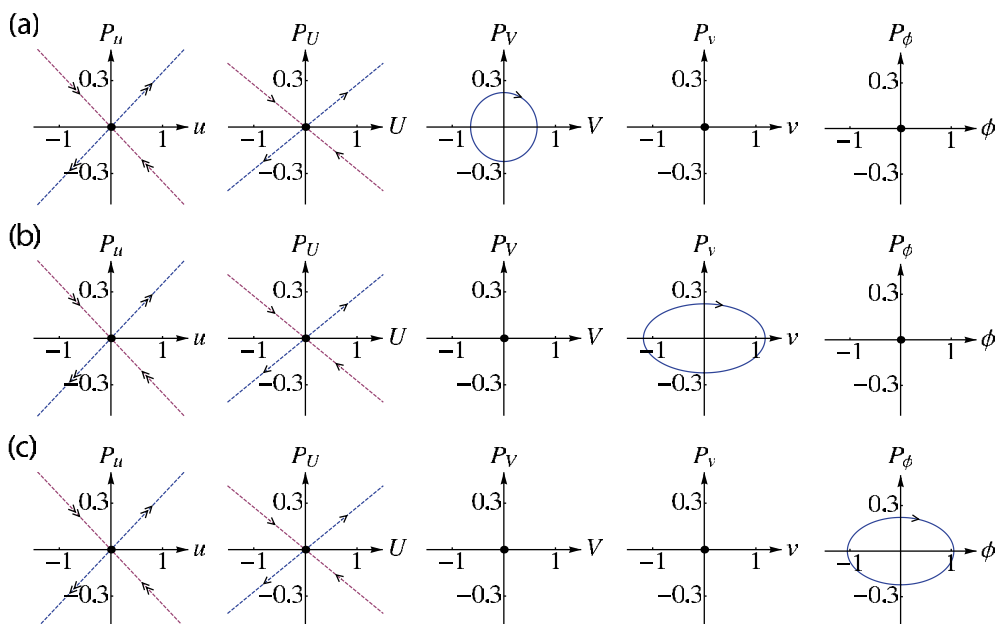


**Figure 10.** The three fundamental modes embedded in the NHIM. These three dynamical modes are shown in normal mode phase space representation: (a) the  $A_1$  normal mode, (b) the  $B_2$  normal mode and (c) the  $B_1$  normal mode.

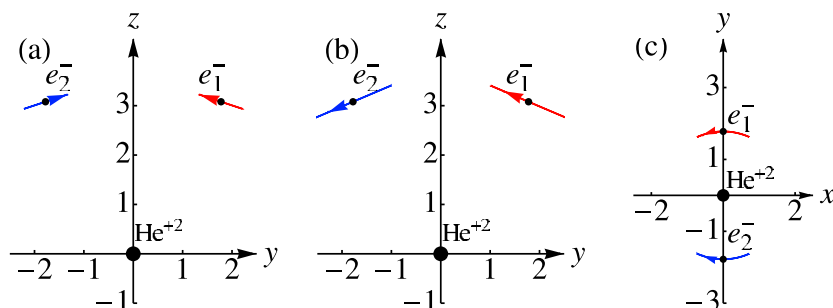


**Figure 11.** The three fundamental modes embedded in the NHIM. These three dynamical modes are shown in the physical coordinates: (a) the  $A_1$  normal mode, (b) the  $B_2$  normal mode and (c) the  $B_1$  normal mode.

the coordinate space dynamics for the stable  $B_1$  mode are shown in figure 11(c). This is the only mode brings the electrons out of the  $yz$ -plane. Note that again, as for the  $A_1$  mode, the momenta are mirror images and consequently the two electrons traverse their periodic orbit in phase with each other.

The generic dynamical behaviour on the NHIM is a combination of these three normal modes. An example is shown in figures 12 and 13. The first of these is the normal mode phase space representation. Again, as the dynamics are confined to the NHIM, the first two modes are confined to their origins. The difference between this and the previous examples are that here all three modes are excited. That is, the dynamics are confined to a three-torus embedded in the NHIM. In figure 13 we see the projections of this three-torus into the  $xy$ -,  $xz$ - and  $yz$ -planes in the physical coordinate space.

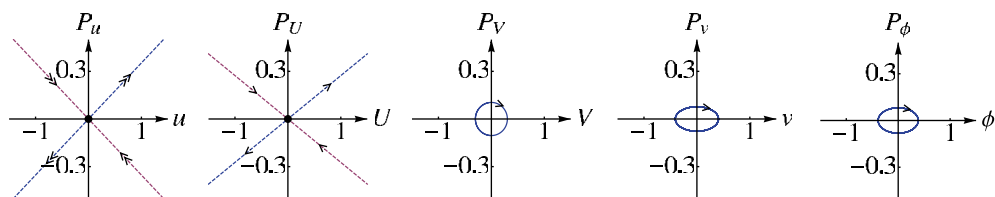


**Figure 12.** A generic trajectory confined to the NHIM shown in the normal mode phase space representation.

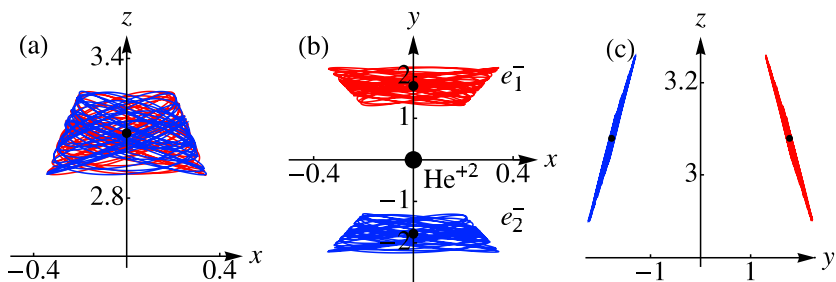


**Figure 13.** The generic trajectory seen in figure 10 shown in the physical coordinates. The trajectories of both electrons are shown in different colours. (a) shows the projections into the  $xz$ -plane, (b) shows the projection into the  $xy$ -plane and (c) shows the projection into the  $yz$ -plane.

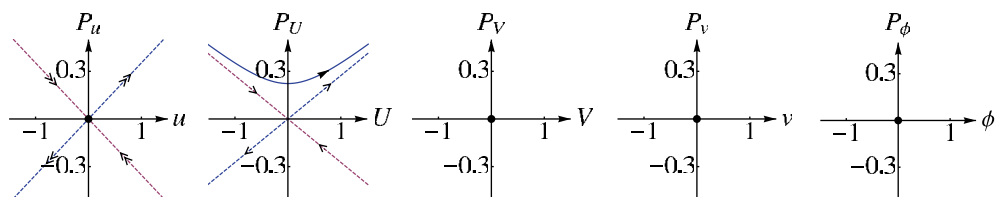


**Figure 14.** The unstable mode  $A_1$  embedded in the pseudo-NHIM shown in the normal mode phase space representation.

**4.4.2. The pseudo-normally hyperbolic invariant manifold.** The pseudo-NHIM,  $\tilde{C}_h$ , is a seven-dimensional invariant manifold embedded in the nine-dimensional energy shell,  $\tilde{\mathcal{E}}_h$ . It is specified by requiring that the action-angle variables of the fast mode be equal to zero,  $I_1 = 0$  and  $\theta_1 = 0$ , subject to the energy requirement  $K(0, I_2, I_3, I_4, I_5) = h$ . This manifold is diffeomorphic to near-critical energy surfaces of a four degree of freedom Hamiltonian with a rank-one saddle.

The dynamics on this surface are confined to invariant manifolds labelled by the four action variables ( $I_2, I_3, I_4, I_5$ ) associated with the four fundamental modes. Three of these are the stable modes discussed just above. The fourth mode corresponds to the slow hyperbolic mode ( $A_1$ ). While the elliptic actions ( $I_3, I_4, I_5$ ) are restricted to positive values, the hyperbolic action  $I_2$  can take both positive and negative values. This mode is shown in figures 14 and 15. In the normal mode picture, figure 14, we see that the system is confined to the origin in all but one mode, the  $A_1$  hyperbolic mode. The projection of this mode into the physical coordinate space is shown in figure 15. This is the mode that corresponds to the non-sequential double ionization; as both electrons cross the saddle point (the dots) they ionize.

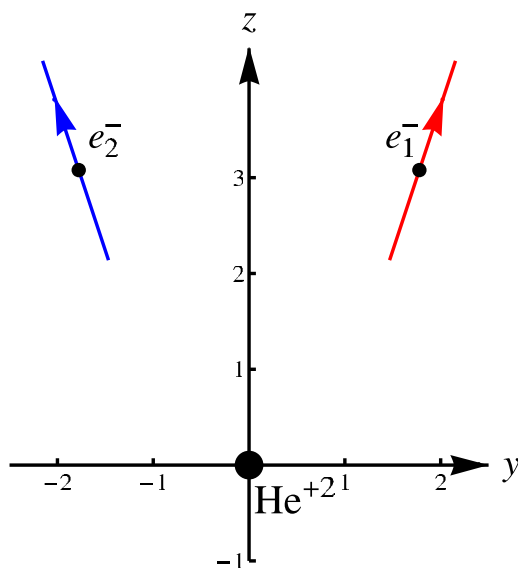


**Figure 15.** The unstable mode  $A_1$  embedded in the pseudo-NHIM shown in the physical coordinates.

In this example the energy in the  $A_1$ -hyperbolic mode has been chosen to be 0.025 hartrees above the saddle point. If energy had been chosen to be below the saddle point ( $I_2 < 0$ ), the system would have been unable to surmount the barrier and both electrons would have been reflected. This is simply an observation that the seven-dimensional pseudo-NHIM can be partitioned into four disjoint volumes. The boundary between these four volumes is a six-dimensional invariant manifold, i.e. codimension one in the seven-dimensional pseudo-NHIM. It can be constructed from the stable and unstable manifolds of the NHIM and is characterized by  $I_1 = 0$ ,  $\theta_1 = 0$ ,  $I_2 = 0$ , and  $K(0, 0, I_3, I_4, I_5) = h$ . This manifold represents an impenetrable barrier for dynamics confined to the pseudo-NHIM. This is illustrated in figures 16 and 17. The difference in initial conditions of the two orbits seen in figure 16 is that they are on opposite sides of the impenetrable barrier. The physical coordinate space orbits are shown in figure 17. Initially the two trajectories are indistinguishable, however as they approach the saddle point the slight difference in the initial conditions make their impact and one of the orbits crosses the saddle point while the second is reflected. This is simply an observation, as noted above, that the pseudo-NHIM is diffeomorphic to near-critical energy surfaces of a four degree of freedom Hamiltonian with a rank-one saddle.

In summary, the dynamics on the pseudo-NHIM are confined to invariant manifolds that can be labelled by the values of the four action variables ( $I_2, I_3, I_4, I_5$ ) subject to the energy condition,  $K(0, I_2, I_3, I_4, I_5) = h$ . The two orbits shown in figures 16 and 17 clearly show that the pseudo-NHIM can be partitioned into distinct volumes associated with ionizing dynamics and non-ionizing dynamics. The boundary between these volumes is given by the condition  $I_2 = 0$ . Clearly, this surface is of codimension one and consequently partitions the pseudo-NHIM into dynamically distinct regions.

**4.4.3. The stable and unstable manifolds of the pseudo-NHIM and the transition state.** The pseudo-NHIM  $\tilde{C}_h$  possesses both stable  $W^s(\tilde{C}_h)$  and unstable  $W^u(\tilde{C}_h)$  manifolds. As

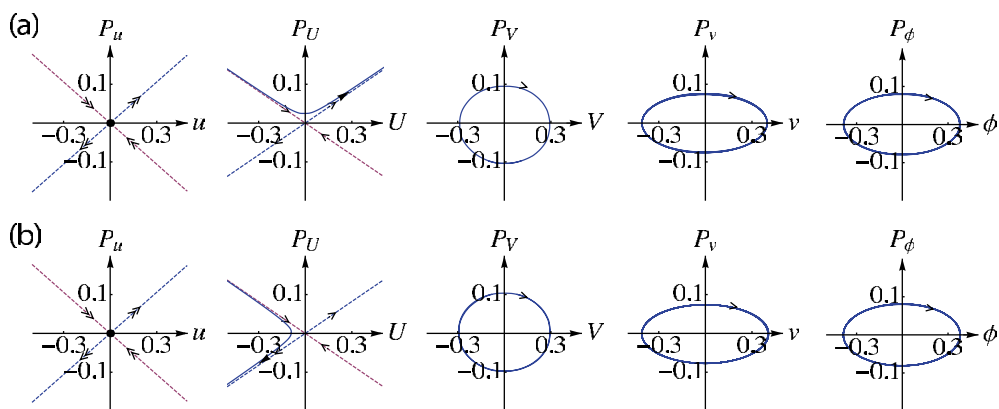


**Figure 16.** Two trajectories embedded in the pseudo-NHIM shown in the normal mode phase space representation. The initial conditions are chosen to be near identical but on opposite sides of the separatrix in the  $P_U$ - $U$  phase space. Trajectory (a) passes over the saddle and ionizes, while trajectory (b) does not have sufficient energy in the  $U$ -mode to surmount the barrier and is reflected.

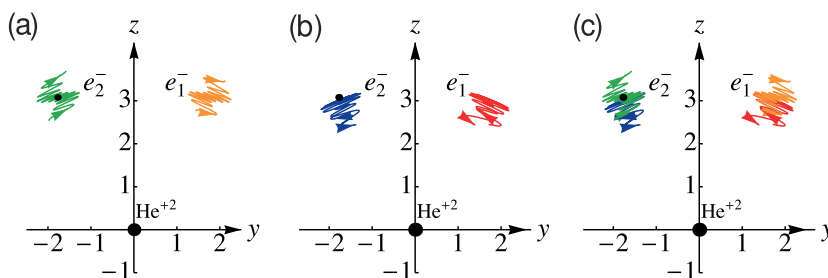


**Figure 17.** Two trajectories seen in figure 15 shown in the physical coordinates. The trajectories of the two electrons are shown in different colours. Trajectory (a) passes over the saddle and ionizes, while trajectory (b) does not have sufficient energy in the  $U$ -mode to surmount the barrier and is reflected, (c) a superposition of the two trajectories illustrating that they can only be distinguished after approaching the transition state.

the pseudo-NHIM is seven-dimensional, its manifolds and the transition state will be eight-dimensional, and thus, of codimension one in the nine-dimensional energy shell  $\tilde{\mathcal{E}}_h$ . Moreover, as both of the manifolds are invariant, they represent impenetrable barriers in the energy shell. They can be partitioned into forward and backward parts,  $W_f^j(\tilde{\mathcal{C}}_h)$  and  $W_b^j(\tilde{\mathcal{C}}_h)$  where  $j = s$  or  $u$ . The union of the forward (backward) parts of the two manifolds yields the forward (backward) reactive tube  $W_f(\tilde{\mathcal{C}}_h) = W_f^s(\tilde{\mathcal{C}}_h) \cup W_f^u(\tilde{\mathcal{C}}_h)$  ( $W_b(\tilde{\mathcal{C}}_h) = W_b^s(\tilde{\mathcal{C}}_h) \cup W_b^u(\tilde{\mathcal{C}}_h)$ ) [26–33]. All states confined inside the forward (backward) reactive tube cross the saddle point and are said to ‘react’.

The flux through the forward and backward reactive tubes is of fundamental physical interest. It can be calculated by constructing any cross-sectional surface of the reactive tube and calculating the flux across the surface. The most convenient manner to accomplish this is to construct a surface of no return, that is, one which is transverse to the flow through the reactive tube (except at the boundary). The forward and backward transition states, defined as

$$\text{TS}_f(\tilde{\mathcal{C}}_h) = \{(I, \theta) : K(I_1, I_2, I_3, I_4, I_5) = h > 0, \theta_1 = 0, I_1 \geq 0\},$$

$$\text{TS}_b(\tilde{\mathcal{C}}_h) = \{(I, \theta) : K(I_1, I_2, I_3, I_4, I_5) = h > 0, \theta_1 = 0, I_1 \leq 0\},$$

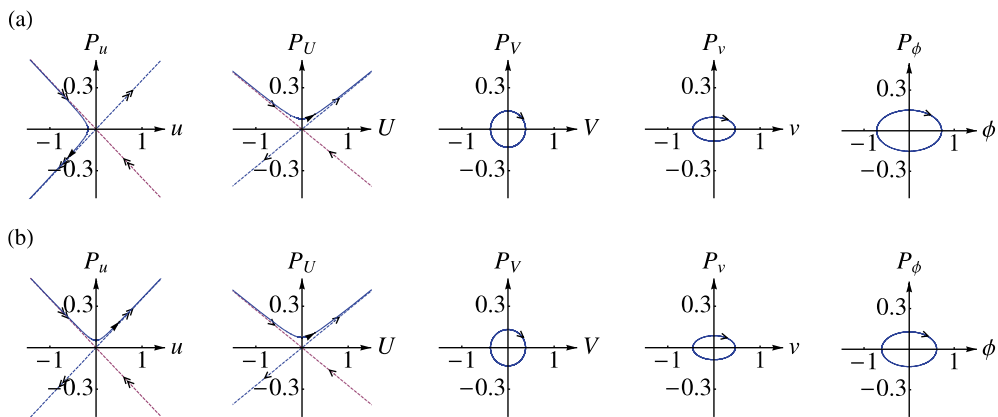


**Figure 18.** Two trajectories embedded in the the energy shell. The initial conditions of these two trajectories are chosen to be near identical. The difference being that they are on opposite sides of the unstable manifold of the pseudo-NHIM. Trajectory (a) has sufficient energy in the  $B_2$  to surmount the barrier, while that seen in (b) does not have sufficient energy and is reflected.

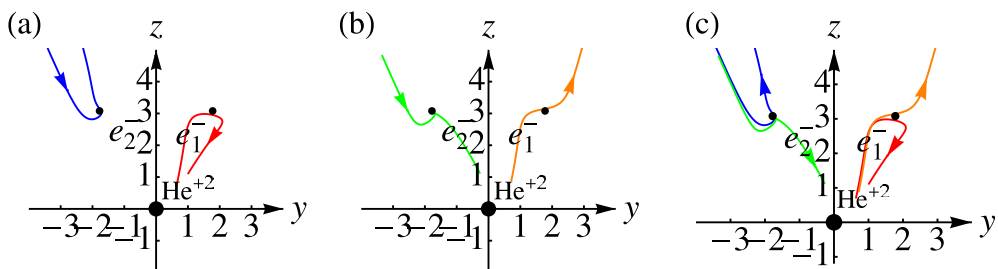


**Figure 19.** The two trajectories seen in figure 18 shown in the physical variables. Trajectory (a) has sufficient energy in the  $B_2$  to surmount the barrier, while that seen in (b) does not have sufficient energy and is reflected, (c) a superposition of the two trajectories illustrating that they can only be distinguished after approaching the transition state.

are such surfaces. They are also codimension one surfaces and partition the energy shell into reactant and product volumes. They are not invariant, and the reaction is said to occur when the system crosses these surfaces.

The relationships between these three codimension one surfaces are illustrated in figures 18 and 19. In figure 18 we see the normal mode representation. These three surfaces have the pseudo-NHIM in common, that is, all possible partitions of the energy among the three elliptic modes and the slow hyperbolic mode are allowed. The difference between these three surfaces occurs in the phase space associated with the fast ( $B_2$ ) hyperbolic mode. In this figure the stable manifold is shown in red, the unstable is blue. The transition state bisects the stable and unstable manifolds of the fast hyperbolic direction. Also shown in this figure are two trajectories whose initial conditions are chosen to be on opposite sides of the stable manifold (red). We see that as the orbits approach the saddle point the one is reflected and the other passes through the transition state as it passes above the saddle point.

Finally, these two trajectories are also shown in the physical coordinate space in figure 19. Again we see that as the two electrons approach the transition state (one from one side and the other from the other side) that in the first case they pass over the saddle point and in the other are reflected by the barrier.

## 5. Summary

We have generalized the theory of rank-one saddles to rank- $m$  ( $m \geq 2$ ) saddles. The generalization is not straightforward as the stable and unstable manifolds of the NHIM are not of codimension one in the energy shell. To make progress one must revert to the theory of pseudo manifolds and use them to extend the NHIM. We call this extended manifold the pseudo-NHIM. The stable and unstable manifolds of the pseudo-NHIM are surfaces of codimension one and, consequently, they partition the energy shell. Once these manifolds are constructed, it is straightforward to define the transition state which in turn can be used to formulate a theory of transport.

We have applied these ideas to a simple but important physical system: the two-electron atom. This model system is of considerable current interest as recent developments in laser spectroscopy enables atomic and molecular physicists to interrogate physical systems at energies in the vicinity of a rank-two saddle. We expect the results presented here will have a significant impact in the interpretation of these results.

Other interesting applications where rank- $m$  saddles occur abound. Two additional examples include astrophysics, the restricted three-body problem which takes into account the attitude of the primaries [66], and chemical reactions, the role of floppy modes in reaction dynamics [67].

## Acknowledgments

The hospitality of Telluride Science Research Center, where this project was originated, is acknowledged. TU acknowledges support from the NSF. JP and PY acknowledge partial support from Project MTM2008-03818/MTM. GH was supported by AFOSR grant FA 9550-06-0092.

## Appendix A. Transformation to normal form for rank- $m$ saddles

In this appendix we address the issue of transforming to normal form in the general case of a rank- $m$  saddle. As a starting point we assume that we have transformed to a set of canonical variables such that the Hamiltonian has the form  $H = H_2 + \sum_{k=3} H_k$  where

$$H_2(P, Q) = \sum_{i=1}^m \lambda_i P_i Q_i + \iota \sum_{i=m+1}^n \omega_i P_i Q_i. \quad (\text{A.1})$$

The higher-order terms  $H_k$ , for  $k = 3, 4, \dots$ , are homogeneous polynomials of degree  $k$  in the variables  $P_i$  and  $Q_i$ 's. Methods for transforming the Hamiltonian into this form are well known and the reader is referred to Laub and Meyer [37] and Meyer *et al* [38] for details.

Our goal is to transform the higher-order terms  $H_k$  into normal form via a nonlinear canonical transformation. We start by defining the Poisson brackets of two functions  $\mathcal{M}$  and  $\mathcal{N}$  that depend on  $P_i^\dagger$  and  $Q_i^\dagger$ 's as  $\{\mathcal{M}, \mathcal{N}\} = \sum_{i=1}^n (\partial \mathcal{M} / \partial Q_i^\dagger) (\partial \mathcal{N} / \partial P_i^\dagger) - (\partial \mathcal{M} / \partial P_i^\dagger) (\partial \mathcal{N} / \partial Q_i^\dagger)$ . Now, if the Lie operator associated with  $H_2$  is given by  $\mathcal{L}_{H_2}(\cdot) = \{\cdot, H_2\}$ , a function  $X$  is said to be in normal form with respect to  $H_2$  if  $\mathcal{L}_{H_2}(X) = 0$ . We pick a monomial of degree  $\ell$  (we take  $\ell \geq 3$ ) given by

$$z_\ell = \alpha P_1^{\dagger k_1} \dots P_n^{\dagger k_n} Q_1^{\dagger j_1} \dots Q_n^{\dagger j_n}$$

where  $\alpha$  is a non-null real or complex constant and  $\sum_{i=1}^n (j_i + k_i) = \ell$  (with  $j_i$  and  $k_i$ 's non-negative integers), we have that

$$\{z_\ell, H_2\} = \left( \sum_{i=1}^m (j_i - k_i) \lambda_i + \iota \sum_{i=m+1}^n (j_i - k_i) \omega_i \right) z_\ell = (\beta_1 + \iota \beta_2) z_\ell. \quad (\text{A.2})$$

The fact that  $H_2$  is semisimple implies that the Lie operator  $\mathcal{L}_{H_2}$  is semisimple and the image of a monomial of degree  $\ell$  is another monomial proportional to it, with proportional constant  $\beta_1 + \iota \beta_2$ . Moreover, because of the semisimple character of  $\mathcal{L}_{H_2}$ , it is straightforward to identify the kernel and the image of  $\mathcal{L}_{H_2}$ : a monomial  $z_\ell$  belongs to  $\ker \mathcal{L}_{H_2}$  if and only if  $\beta_1 = \beta_2 = 0$ , otherwise it belongs to  $\text{im } \mathcal{L}_{H_2}$ .

Thus, given a homogeneous polynomial of degree  $\ell$ , say  $Y_\ell$ , it is composed by the sum of monomials of the type  $z_\ell$ . To put  $Y_\ell$  in normal form means to split it into two parts, one belonging to  $\ker \mathcal{L}_{H_2}$  and the other that belongs to  $\text{im } \mathcal{L}_{H_2}$ . We proceed term by term of  $Y_\ell$ . So, once  $z_\ell$  is picked, if  $\beta_1 = \beta_2 = 0$ , we keep it in the transformed Hamiltonian (i.e. in the normal-form Hamiltonian) but if  $\beta_1 \neq 0$  or  $\beta_2 \neq 0$  we incorporate the monomial  $(-1/(\beta_1 + \iota \beta_2)) z_\ell$  to the generating function. Thus, we build the normal-form Hamiltonian,  $K_\ell$ , and the generating function  $\mathcal{W}_\ell$  related to  $Y_\ell$  by checking the conditions of (A.2) for all the monomials that  $Y_\ell$  is made of. By construction,  $K_\ell$  and  $\mathcal{W}_\ell$  are homogeneous polynomials of degree  $\ell$  and  $Y_\ell = \mathcal{L}_{H_2}(\mathcal{W}_\ell) + K_\ell$  as we have split  $Y_\ell$  into terms of the kernel and of the image of  $\mathcal{L}_{H_2}$ .

The procedure is iterated over the degree  $\ell$  of the polynomials, so that, in the next step, the Hamiltonian of degree  $\ell + 1$  is handled in the same way as we explained for the degree  $\ell$ . However, in order to advance from degree  $\ell$  to degree  $\ell + 1$  one needs to compute a sequence of intermediate Hamiltonians using the generating functions up to degree  $\ell$  and the recurrences provided by the Lie triangle, as is customary in normal-form transformations. This is achieved using the Lie–Deprit method [64], and the entire process is carried out to the desired degree  $N$ . As a result of the transformation one constructs the normal-form Hamiltonian,  $K = K_2 + \dots + (1/(N-2)!)K_N$ , together with the generating function  $\mathcal{W} = \mathcal{W}_3 + \dots + (1/(N-3)!) \mathcal{W}_N$ . We note that  $K_2 \equiv H_2$  and one starts at degree 3 (order 1) and ends up at degree  $N$  (order  $N-2$ ). Thus the normal-form transformation consists of  $N-2$  steps. The final steps consists in calculating explicitly the forward and backward normal-form transformations using  $\mathcal{W}$  and some recurrence formulas based on Lie triangles.

A sufficient condition for a given monomial to belong to  $\ker \mathcal{L}_{H_2}$  is that  $j_i = k_i$  for  $i = 1, \dots, n$ . There could be other combinations of the  $\lambda_i$  and  $\omega_i$ 's such that  $\beta_1 = \beta_2 = 0$ . (Observe that the  $\lambda_i$ 's cannot be combined with the  $\omega_i$ 's to get a monomial in the kernel of  $\mathcal{L}_{H_2}$ .) These combinations would lead to resonances and would appear when some of the possible ratios  $\lambda_i/\lambda_j$  are rational (or the ratios  $\omega_i/\omega_j$  are rational). However, in many practical applications the frequencies are incommensurate as is the case of the example of this paper.

By construction, in the absence of resonances the normal-form Hamiltonian depends on the transformed variables,  $P_1^\dagger, \dots, P_n^\dagger, Q_1^\dagger, \dots, Q_n^\dagger$  only through the products  $P_1^\dagger Q_1^\dagger, \dots, P_n^\dagger Q_n^\dagger$ . This is a simple fact derived from (A.2). Indeed, in order to get the terms of  $K_\ell$ , for each monomial  $z_\ell$  of  $Y_\ell$  one needs that  $j_i = k_i$  for  $i = 1, \dots, n$ , so the only terms kept on  $K_\ell$  are those monomials of the form  $\alpha (P_1^\dagger Q_1^\dagger)^{j_1} \dots (P_n^\dagger Q_n^\dagger)^{j_n}$ . This situation is ideal from the point of view of the simplicity of the transformation to normal form. Indeed, once the higher-order terms are truncated, the resulting Hamiltonian has all its  $n$  degrees of freedom decoupled, therefore, it has  $n$  (real) integrals of motion  $I_1 = P_1^\dagger Q_1^\dagger, \dots, I_m = P_m^\dagger Q_m^\dagger, I_{m+1} = \iota P_{m+1}^\dagger Q_{m+1}^\dagger, \dots, I_n = \iota P_n^\dagger Q_n^\dagger$ . By inverting the integrals of motion  $I_1, \dots, I_n$ ,

(possibly together with the rest of linear changes needed to put the quadratic part into normal form), one obtains approximate integrals of motion for the initial Hamiltonian, that is, functions  $I_1^*, \dots, I_n^*$  that are approximate integrals of  $H$  in a neighbourhood where the normal-form approach is valid.

Nevertheless it can occur that at a certain degree, the quantities  $\beta_1$  and  $\beta_2$  become close to zero, therefore the coefficients of the generating function and the Hamiltonians at higher degrees become large. This is the well known case of the appearance of small denominators. The effect of these terms is the divergence of the transformations—in general the normal-form transformations are divergent but can behave nicely in a neighbourhood of the rank- $m$  saddle. The greater the degree  $\ell$  is, the higher the probability that  $\beta_1$  and  $\beta_2$  become smaller. In the application we show a couple of procedures to check that the generating function and the normal-form Hamiltonian behave well in a neighbourhood of the fixed point and can be used to make valuable simulations, even when their coefficients increase with the degree of the expressions.

If resonances play a role in the Hamiltonian, it is no longer possible to decouple the  $n$  degrees of freedom. The number of integrals that can be obtained after truncating the tail of the normal form depend on the number of ratios  $\lambda_i/\lambda_j$  and  $\omega_i/\omega_j$  that are rational. In the context of the present work we need at least to decouple the degree of freedom related to the largest eigenvalue  $\lambda_1$ . Thus, we would require that the ratios  $\lambda_1/\lambda_j$  with  $j = 2, \dots, m$  are not positive rationals or close to them. Then, the quantity  $I_1 = P_1^\dagger Q_1^\dagger$ , would become an integral of motion, regardless of the rest of hyperbolic and elliptic directions. By doing so the Hamiltonian function is in the required form by the theory of section 3.

## References

- [1] Wiggins S, Wiesenfeld L, Jaffé C and Uzer T 2001 Impenetrable barriers in phase-space *Phys. Rev. Lett.* **86** 5478–81
- [2] Uzer T, Jaffé C, Palacián J, Yanguas P and Wiggins S 2002 The geometry of reaction dynamics *Nonlinearity* **15** 957–92
- [3] Jaffé C, Kawai S, Palacián J, Yanguas P and Uzer T 2005 A new look at the transition state: Wigner's dynamical perspective revisited *Adv. Chem. Phys.* **130A** 171–216
- [4] Murrell J N and Laidler K J 1968 Symmetries of activated complexes *Trans. Faraday Soc.* **64** 371–7
- [5] Wales D J and Berry R S 1992 Limitations of the Murrell–Laidler theorem *J. Chem. Soc. Faraday Trans.* **88** 543–4
- [6] Heidrich D and Quapp W 1986 Saddle points of index 2 on potential energy surfaces and their role in theoretical reactivity investigations *Theor. Chim. Acta* **70** 89–98
- [7] Mezey P G 1987 *Potential Energy Hypersurfaces* (Amsterdam: Elsevier)
- [8] Cavagna A, Giardini I and Parisi G 2001 Role of saddles in mean-field dynamics above the glass transition *J. Phys. A: Math. Gen.* **34** 5317–26
- [9] Wales D J 2003 *Energy Landscapes* (Cambridge: Cambridge University Press)
- [10] Wales D J and Doye J P K 2003 Stationary points and dynamics in high-dimensional systems *J. Chem. Phys.* **119** 12409–16
- [11] Eyring H and Polanyi M 1931 Über einfache Gasreaktionen *Z. Physik. Chem. B* **12** 279–311
- [12] Wigner E P 1938 The transition state method *Trans. Faraday Soc.* **34** 29–40
- [13] Keck J C 1967 Variational theory of reaction rates *Adv. Chem. Phys.* **XIII** 85–121
- [14] Pechukas P 1981 Transition state theory *Annu. Rev. Phys. Chem.* **32** 159–77
- [15] Truhlar D G, Hase W L and Hynes J T 1983 Current status of transition-state theory *J. Phys. Chem.* **87** 2664–82
- [16] Truhlar D G, Garrett B C and Klippenstein S J 1996 Current status of transition-state theory *J. Phys. Chem.* **100** 12711
- [17] Jaffé C, Ross S D, Lo M W, Marsden J, Farrelly D and Uzer T 2002 Statistical theory of asteroid escape rate *Phys. Rev. Lett.* **89** 011101
- [18] Jaffé C and Uzer T 2004 On the occurrence of transition states in celestial mechanics *Ann. New York Acad. Sci.* **1017** 39–45